

A three-part-quantile bias correction with spatial transfer for the correction of simulated European river runoff to force ocean models

Stefan Hagemann*, Thao T. Nguyen and Ha T. M. Ho-Hagemann

Institute of Coastal Systems – Analysis and Modelling, Helmholtz-Zentrum Hereon, Max-Planck-Str. 1, 21502 Geesthacht, Germany

*Correspondence: Dr. Stefan Hagemann, stefan.hagemann@hereon.de

1 Abstract

2 In ocean or Earth system model applications, the riverine freshwater inflow is an important flux
3 affecting salinity and marine stratification in coastal areas. However, in climate change studies,
4 the river runoff based on climate model output often has large biases on local, regional or even
5 basin-wide scales. If these biases are too large, the ocean model forced by the runoff will drift
6 into a different climate state compared to the observed state, which is particularly relevant for
7 semi-enclosed seas such as the Baltic Sea. To achieve low biases in riverine freshwater inflow
8 in large-scale climate applications, a bias correction is required that can be applied in periods
9 where runoff observations are not available and that allows spatial transferability of its
10 correction factors. In order to meet these requirements ~~for low biases in river runoff~~, we have
11 developed a three-part-quantile bias correction that includes different correction factors for low,
12 medium and high percentile ranges of river runoff over Europe. Here, we present an
13 experimental setup using the Hydrological Discharge (HD) model and its high-resolution
14 (1/12°) grid. First, bias correction factors are derived at the locations of the downstream stations
15 with available daily discharge observations for many European rivers. These factors are then
16 transferred to the respective river mouths and mapped to neighbouring grid boxes belonging to
17 ungauged catchments. The results show that the bias correction generally leads to an improved
18 representation of river runoff. Especially over Northern Europe, where many rivers are
19 regulated, the three-part-quantile bias correction provides an advantage compared to a bias
20 correction that only corrects the mean bias of the river runoff. Evaluating two NEMO ocean
21 model simulations in the German Bight indicated that the use of the bias corrected discharges
22 as forcing leads to an improved simulation of sea surface salinity in coastal areas. Although in
23 the present study, the bias correction is tailored to the high-resolution HD model grid over
24 Europe, the methodology is suitable for any high-resolution model region with a sufficiently
25 high coverage of river runoff observations. It is also noted that the methodology is applicable
26 to river runoff based on climate hindcasts as well as on historical climate simulations where the
27 sequence of weather events does not match the actual observed history. Therefore, it may also
28 be applied in climate change simulations.

29 **Keywords:** Bias correction, river runoff, discharge, high resolution, Europe, sea-surface
30 salinity

31

32

33 1 Introduction

34 River runoff (or discharge/streamflow) is an important component of the global hydrological
35 cycle, accounting for about one-third of precipitation over land areas. It closes the water cycle
36 between land and ocean and influences various ocean properties, in particular the salinity of
37 coastal and semi-enclosed seas (e.g. Väli et al., 2013), the ocean stratification in shelf areas
38 (e.g. Hordoir and Meier, 2010) such as the German Bight (Becker et al., 1992), and the
39 thermohaline circulation in different regions (e.g. Hordoir et al., 2008; Lehmann and
40 Hinrichsen, 2000; Marzeion et al., 2007). In addition, river runoff and associated nutrient loads
41 are important factors influencing marine ecosystem functioning (Daewel and Schrum, 2017).

42 Consequently, river runoff needs to be adequately represented in studies of the impacts of
43 climate change on the marine environment or in coupled Earth system studies. In such studies,
44 the atmospheric data used to force the respective ocean model are usually taken from climate
45 models, reanalysis products or hydrological models. Here, it is desirable that the river runoff is
46 consistent with the atmospheric forcing (e.g. Vinayachandran et al., 2015; Hagemann and
47 Stacke, 2022), i.e. that the impact of weather events and trends in the atmospheric forcing is
48 transferred via the river runoff into the ocean. In previous modelling studies, runoff was often
49 taken from climatology or discharge observations, especially when hindcasts were used.
50 However, this is not a recommended approach for climate change studies where consistently
51 simulated river runoff should be used. Runoff from the driving climate, land surface or
52 hydrological model will contain biases, e.g., due to biases in precipitation and/or uncertainties
53 in the land surface representation of the model. Many simulations of historical daily river runoff
54 show common biases in the tails of their distributions, with high discharges underestimated and
55 low discharges overestimated (Farmer et al., 2018, and references therein). If the basin-wide
56 biases are too large, a bias correction of the simulated discharge would be necessary to avoid
57 the ocean model drifting into a different climate state compared to the observed state. This is
58 particularly relevant for semi-enclosed seas such as the Baltic Sea. For example, for Baltic Sea
59 ocean models, the mean long-term bias of river runoff must be less than 7% (Hagemann and
60 Stacke, 2022).

61 The bias correction of river runoff is an approach that has been used particularly for short-
62 term hydrological forecasts and ensemble predictions of up to six months. Here, Kim et al.
63 (2021) provide examples of related studies. However, these approaches (see, e.g., those listed
64 in Kim et al., 2021; Madadgar et al., 2014) are often specifically trimmed to flood forecasts.
65 Therefore, they often require the existence of observed values from previous time steps so that
66 that are not applicable in climate change studies, such as autoregression models (Kim et al.,
67 2021) or components of a Bayesian forecasting system (Krzysztofowicz and Maranzano, 2004).
68 Others like non-parametric methods based on Bayesian approaches as proposed by Brown and
69 Seo (2010; 2012) need a large number of ensemble members (Madadgar et al., 2014).

70 Recently, bias correction of river runoff has also been applied in the context of climate
71 change. Quantile mapping based approaches are often used for such bias correction, as this
72 usually leads to a large improvement in the representation of discharge of the considered river.
73 For example, Budhathoki et al. (2022) used quantile mapping to correct discharge bias in the
74 Chao Phraya River basin (Thailand), and Daraio (2020) used it for two basins in New Jersey
75 (USA). A criticism of using quantile-mapping in flood forecasting is that it does not maintain
76 the pairing of corresponding simulated and observed flows (Madadgar et al., 2014). However,
77 Madadgar et al. (2014) also noted that quantile mapping was not always successful in improving
78 the initial forecast trajectory. In their application for the Sprague River (southern Oregon,

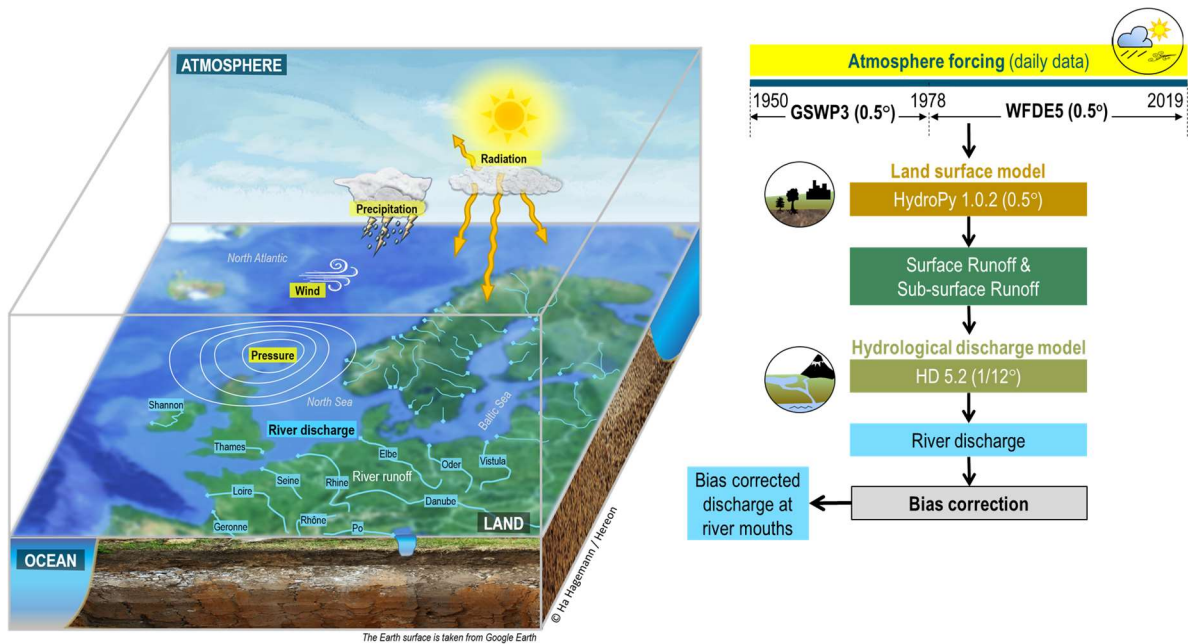
79 USA), the skill of the forecast actually deteriorated when the quantile mapping technique was
80 used. Similarly, Malek et al. (2022) used a quantile mapping based bias correction of discharge
81 and showed that ex-post corrections of simulated discharge do not necessarily reduce biases in
82 the simulation of key processes and in some cases can severely degrade system simulations.

83 Consequently, the aim of the present study was to develop a bias correction method sufficient
84 to meet the requirements of ocean models in large-scale climate change studies. Note that we
85 did not aim for the most accurate reproduction of observed discharge characteristics, as required
86 for short-term hydrological predictions and flood forecasts used by water resource decision
87 makers (e.g. Shi et al., 2008). In order to maintain a high degree of temporal consistency of
88 simulated runoff with the meteorological patterns in the driving (on- or offline) climate model
89 (or data), a bias correction with as little fitting or modification of the daily sequence of runoff
90 curves as possible is desired. Thus, our target is a simple bias correction that corrects the mean
91 bias and the tail biases of the discharge distribution in climate change applications of ocean or
92 coupled system models. The bias correction factors should be transferable from downstream
93 stations to river mouths as well as to neighbouring ungauged catchments. Furthermore, it should
94 be applicable to climate model or Earth system model data that lack the observed sequence of
95 actual discharge events. Therefore, we decided to not apply methods that employ detailed
96 modifications of the discharge curves for specific rivers such as those methods that use complex
97 matrix arithmetic of observed and simulated discharge time series (e.g. Zhao et al., 2011), or
98 the common quantile-mapping approaches. The latter are conducted using a lot of bins, so that
99 the bias in the discharge curve of a specific river can be strongly reduced. However, these
100 detailed correction factors for every bin may likely not be transferred to other locations. It may
101 work for the same river if station and river mouth are relatively close to each other, but certainly
102 may not be valid for the transfer to neighbouring catchments.

103 The manuscript is organised as follows. Section 2 describes how the simulated discharges
104 were generated and the newly developed bias correction methodology, as well as the data,
105 models and metrics used in this study. Sections 3 and 4 evaluate the simulated and bias corrected
106 discharges and present the effects of the bias correction for station locations and sea basin
107 inflows, respectively. Finally, Section 5 concludes with a summary and conclusions.

108 **2 Data and Methods**

109 To generate the freshwater inflow from rivers to the ocean, we used an experimental setup
110 analogous to Hagemann and Stacke (2022). Here we used two atmospheric forcing datasets
111 (Sect. 2.1) and the same model chain of two large-scale hydrological models. The global
112 hydrological model HydroPy (Sect. 2.2) was used to generate the input to the Hydrological
113 Discharge (HD) model (Sect. 2.3) at the resolution of the atmospheric forcing data (0.5°). These
114 input data of surface and sub-surface runoff were then interpolated onto the HD model grid and
115 the HD model was used to simulate daily discharges from land to sea. Subsequently, we bias
116 corrected these time series as described in Section 2.4 to generate bias corrected discharges at
117 coastal ocean boxes of the European HD model domain from 1901-2019. Note that we
118 combined the simulations based on two different atmospheric forcing datasets to cover the
119 whole 20th century and to include the more recent years in the bias corrected discharge time
120 series. Such an approach was also used in the second phase (ISIMIP, 2023) of the Inter-Sectoral
121 Impact Model Inter-Comparison Project (ISIMIP; Warszawski et al., 2014). Figure 1
122 summarises the experimental setup. Section 2.5 refers to the observational data that are used in
123 the evaluation of the model results. Finally, the evaluation metrics used in the analysis of the
124 results are presented in Sect. 2.7.



125

126

127 **Figure 1.** Overview on the main steps of generating bias corrected river discharge at HD
 128 river mouths.

129

130 2.1 Atmospheric forcing

131 We used two atmospheric datasets comprising daily data of various near-surface atmospheric
 132 variables. They have been used as meteorological forcing datasets in several climate impact
 133 assessments and are recommended by ISIMIP (2023). Both datasets were specifically generated
 134 for foreingto force global hydrological models for hindcast simulations. They are based on re-
 135 analysis products from different weather forecast centres and bias-correction procedures were
 136 applied by the respective creators to improve their data.

137 The Global Soil Wetness Project Phase 3 (GSWP3; Dirmeyer et al., 2006; Kim, 2017)
 138 dataset is available at 0.5° resolution from 1901-2014. To generate the GSWP3 dataset, Kim
 139 (2017) dynamically downscaled the 20th Century Reanalysis (Compo et al., 2011) ~~was first~~
 140 ~~dynamically downscaled~~ onto the T248 (~0.5°) grid using a spectral nudging technique
 141 (Yoshimura and Kanamitsu, 2008) in a Global Spectral Model (~~GSM~~). Observation-based bias
 142 correction procedures were then applied to the downscaled data to obtain daily time series.

143 To generate the WFDE5 dataset, Cucchi et al. (2020) applied the WATCH Forcing Data
 144 (~~WFD~~) methodology (Weedon et al., 2011) ~~was applied~~ to surface meteorological variables
 145 from the ERA5 reanalysis (Hersbach et al., 2020) to obtain bias corrected time series. ERA5 is
 146 the fifth generation of atmospheric reanalysis produced by the European Centre for Medium-
 147 Range Weather Forecasts (ECMWF). WFDE5 is provided at 0.5° spatial resolution from 1979-
 148 2019. Mengel et al. (2021) stated that WFDE5 is considered as the more realistic dataset,
 149 especially with respect to day-to-day variability for variables for which the monthly mean
 150 values were bias corrected, such as precipitation and temperature. For more information on

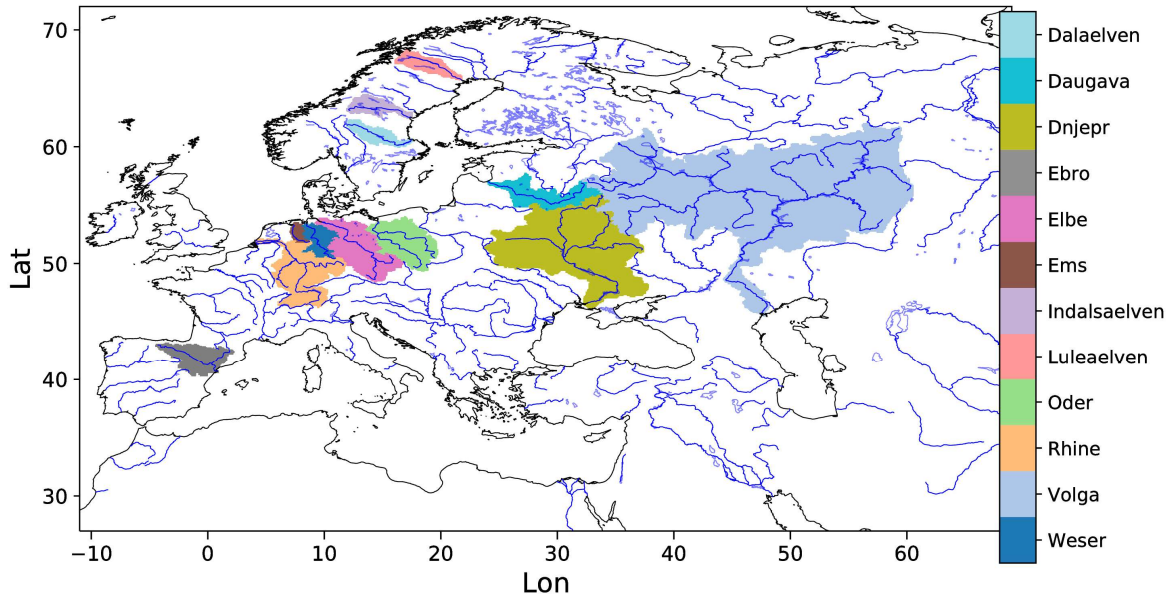
151 application and evaluation of both datasets, see, e.g., Mengel et al. (2021) and references
152 therein, Hassler and Lauer (2021), (Arora et al., 2023).

153 2.2 HydroPy setup

154 HydroPy (Stacke and Hagemann, 2021) is a state-of-the-art global hydrology model for
155 which no model calibration was performed for its setup. Within global hydrological modelling,
156 the usage of uncalibrated models is rather common (see, e.g., Haddeland et al., 2011), even
157 though some models exist that are calibrated for global studies. In the present study, HydroPy
158 was driven by daily forcing data from 1901-2019. Daily input fields of surface and subsurface
159 runoff were generated at a resolution of 0.5°. Analogous to the ERA5 forced simulation in
160 Hagemann and Stacke (2022), precipitation, 2m temperature, downwelling shortwave and
161 longwave radiation, 2m specific humidity, surface pressure and 10m wind are used as forcing
162 from the respective forcing dataset. We performed a spin-up simulation over 50 iterations of
163 the year 1901 with the GSWP3 forcing (cf. Stacke and Hagemann, 2021) to initialize the
164 storages in the HydroPy model and to avoid any drift during the actual simulation period. We
165 then forced HydroPy with the GSWP3 data from 1901-1978 and continued with the WFDE5
166 data from 1979-2019. We also conducted a GSWP3 forced simulation from 1979-2014 in order
167 to derive bias correction parameters for the earlier period. For our analysis, we focus on the
168 years from 1950 onwards so that we have an additional transient spin-up of 49 years.

169 2.3 HD model setup

170 ~~To simulate discharge, t~~The HD model (Hagemann et al., 2020) is a well-established river
171 routing model that is implemented in a range of global and regional model systems. As noted
172 in Hagemann et al. (2020), no river specific parameter adjustments were conducted in the HD
173 model to enable its applicability for climate change studies and over catchments, where no daily
174 discharges are available at a downstream station. To simulate discharge with the HD model, we
175 used the daily input fields of surface and subsurface runoff that were generated by HydroPy
176 from the GSWP3 and WFDE5 data (see Sect. 2.2). As the time step of these runoff data is one
177 day, the time step of the HD model was also set to one day. However, an internal time step of
178 0.5 hours is used for the flow within the river, as the minimum travel time through a grid box
179 is limited by the chosen time step. The HD model v5.2.0 (Hagemann et al., 2023) was applied
180 over the European domain, which covers the land areas between -11°W to 69°E and 27°N to
181 72°N. The domain, along with a number of rivers specifically noted in this study, is shown in
182 Figure 2. In the following, we refer to the WFDE5-based discharges as HD5-WFDE5W and to
183 the GSWP3-based discharges as HDG5-GSWP3. The corresponding bias-corrected discharges
184 are referred to as HD-BC in general and HDW-BC and HDG-BC in particular.



185

186

Figure 2. European HD model domain and catchment areas for selected rivers

187

2.4 Bias correction of river runoff

188

189

190

191

192

193

194

195

196

197

198

199

200

201

We have developed a bias correction method for river runoff that uses correction factors for three quantiles and includes a spatial transfer of these factors. We note that our three-quantile bias correction is similar to a very coarse quantile mapping. The latter has been introduced in climate change impact research to correct for significant biases in data produced by global and regional climate models. Quantile mapping is a distribution mapping in which the distribution function of climate values is corrected to match the observed distribution function. Details of such mapping applied to precipitation and surface air temperature can be found, for example, Piani et al. (2010) and Teutschbein and Seibert (2012). Our bias correction method involves several steps. First, three-part bias correction method for river runoff with different correction factors for low, medium and high percentiles. These are first calculated at the station locations and then applied to-at the respective river mouths. Finally, an interpolation is performed to neighbouring coastal mouth points for which no downstream observations are available in the respective catchment. This procedure is summarised in Figure 3. The three percentile ranges for daily discharge q_i are classified by

202

203

204

- Low (L): $q_i \leq Q_p$
- Medium (M): $Q_p < q_i < Q_{100-p}$
- High (H): $q_i \geq Q_{100-p}$

205

206

207

208

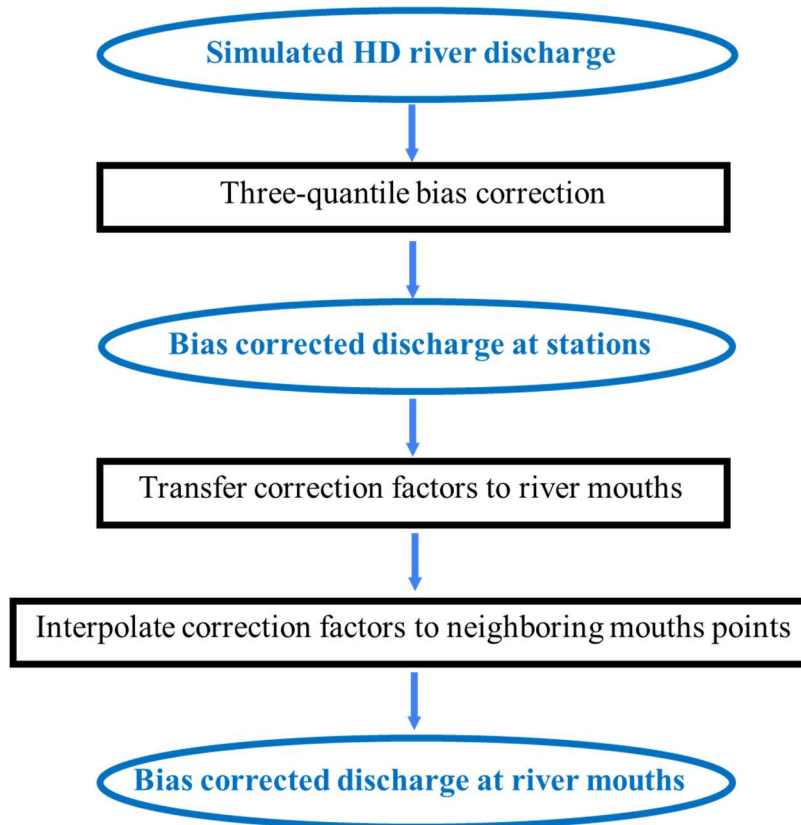
209

210

Here, Q_p denotes the p^{th} percentile of the daily discharge and p was set to 20. The percentiles Q_p and Q_{100-p} were determined separately for the observed and the simulated discharges at the downstream station locations and then the mean discharges \bar{q}_R were calculated for the three percentile ranges $R \in \{L, M, H\}$. Note that for these calculations only those days were considered for which an observed discharge was available. Then, the mean bias b_R (in %) was calculated for each percentile range and a correction factor f_R to remove the bias was derived as

211

$$f_R = \frac{100}{b_R + 100}$$



213

214 **Figure 3.** Steps to derive bias corrected discharge at river mouths from simulated
 215 discharges.

216 For the evaluation of the bias correction in Sect. 3, these correction factors were applied to
 217 the simulated discharges at the station locations. As the correction factors are independent of
 218 the absolute amount of discharge, they could be applied to the respective river mouths. For each
 219 river mouth with more than one inflow ($j > 1$) for which a correction factor $f_{R,j}$ is determined, a
 220 combined correction factor is obtained by calculating an average weighted by the respective
 221 mean inflows Q_j .

222

$$\bar{f}_R = \frac{\sum_j f_{R,j} * Q_j}{\sum_j Q_j}$$

223 From these river mouths, an interpolation is performed to neighbouring coastal mouth points
 224 for which no downstream observations are available in the respective catchment. This
 225 interpolation was motivated by the fact that the general pattern of bias of neighbouring rivers
 226 is often similar (cf. Sect. 3.1). The interpolation is performed by inverse distance weighting
 227 from the four closest (or fewer) river mouths within a search radius of 200 km. If no river mouth
 228 with a correction factor was found within the search radius, the correction factor was set to one
 229 (i.e. no correction).

230 Note that the bias correction can lead to spurious daily jumps in discharge when the
 231 percentile boundary is crossed and the bias correction factors differ between the percentile

232 ranges. In order to reduce this effect, a smoothing radius of $\Delta s = 0.05$ was introduced around
 233 the percentile boundaries, which was applied at both station locations and river mouths.

234 For $(1 - \Delta s) * \varphi Q_p < q_i < (1 + \Delta s) * \varphi Q_p$:

$$235 \quad \tilde{q}_i = q_i * (f_L + (f_M - f_L)) * \frac{(q_i - (1 - \Delta s) * \varphi Q_p)}{2 * \Delta s * \varphi Q_p}$$

236 For $(1 - \Delta s) * \varphi Q_{100-p} < q_i < (1 + \Delta s) * \varphi Q_{100-p}$:

$$237 \quad \tilde{q}_i = q_i * (f_M + (f_H - f_M)) * \frac{(q_i - (1 - \Delta s) * \varphi Q_{100-p})}{2 * \Delta s * \varphi Q_{100-p}}$$

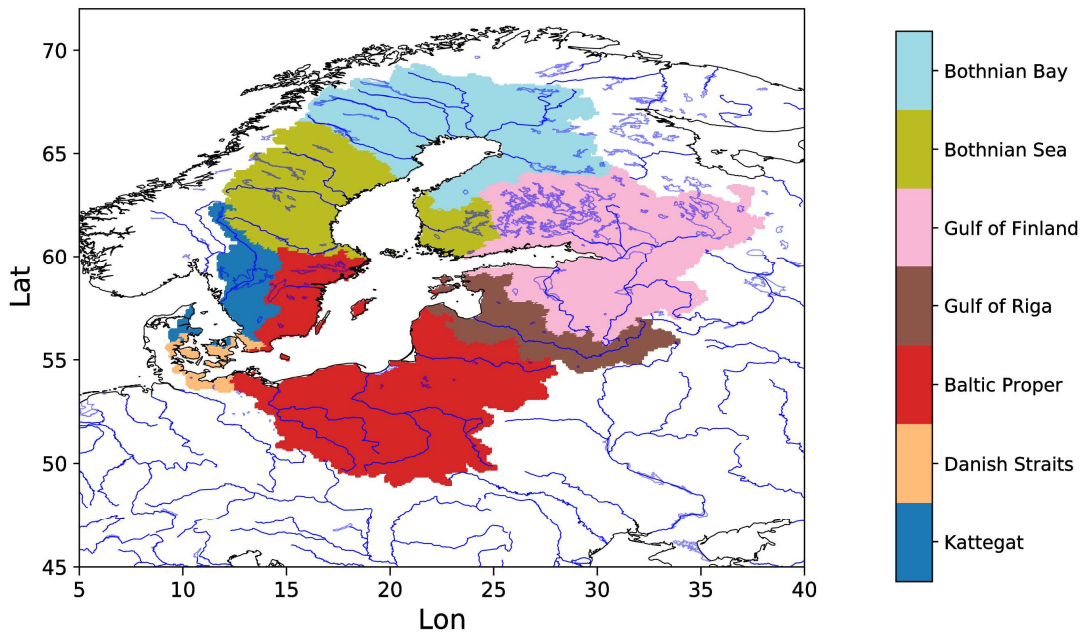
238 The bias correction procedure corrects the days that fall into the different percentile ranges.
 239 However, this does not necessarily mean that it also corrects the whole distribution into the
 240 three percentile ranges. Particularly, if the biases in these ranges are quite different, the days
 241 may change their class and order within the distribution.

242 In order to apply the three-part-quantile bias correction to the simulated discharge time series
 243 from 1901-2019, two sets of bias correction factors were derived. The first set uses HD~~WS-~~
 244 ~~WFDES~~ and discharge station observations for the period 1979-2014. This set was used to bias
 245 correct the simulated discharge at HD river mouths from 1979-2019. The second set uses a
 246 further discharge simulation where we continued HD~~G5-GSWP3~~ utilizing the GSWP3 forcing
 247 up to 2014. Again, the set of bias correction factors was derived for the period 1979-2014 using
 248 discharge station observations. This set was then used to bias correct the simulated discharge at
 249 the HD river mouths from 1901-1978.

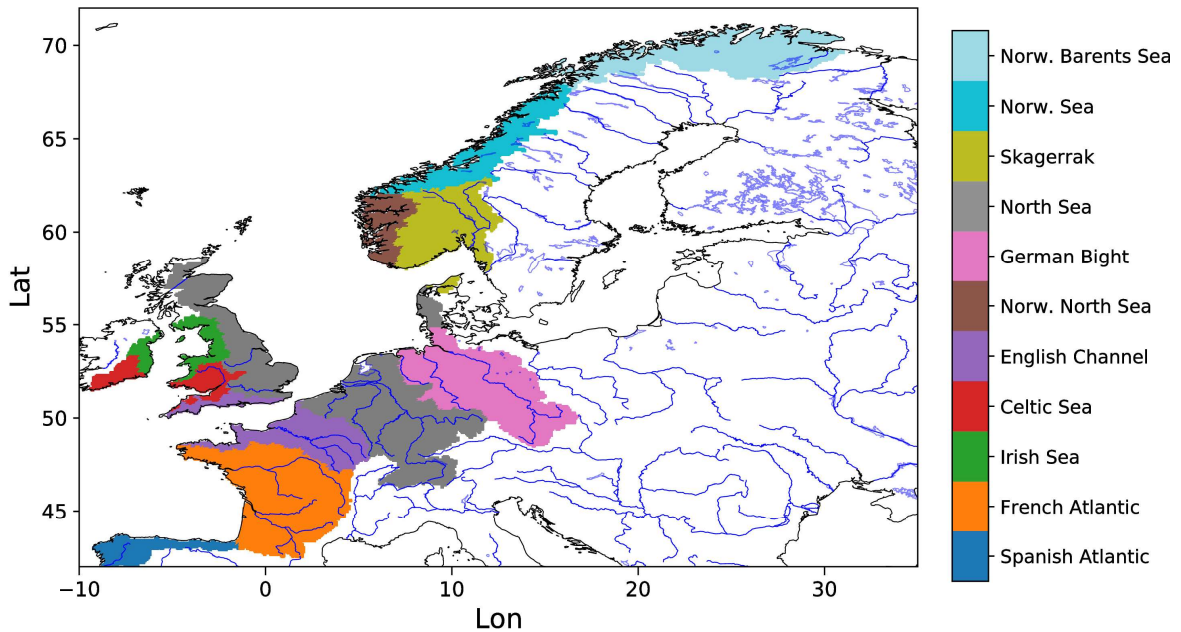
250 2.5 Observed discharge data

251 We used available daily discharge data from downstream gauges for many rivers across Europe
 252 with a catchment area of about 1000 km² or more. These station data were obtained from Global
 253 Runoff Data Centre (~~GRDC~~) and various agencies and institutions listed in table 2 of Hagemann
 254 and Stacke (2022). In addition, French discharge data were accessed from the E.U. Copernicus
 255 Marine Service Information. In order to allow an assessment of the discharge at the river
 256 mouths, we considered basin-wide estimates from three different sources.

257 For the Baltic Marine Environment Protection Commission – also known as the Helsinki
 258 Commission (HELCOM), Svendsen and Gustafsson (2022) provided annual waterborne
 259 inflows into the seven main sub-basins of the Baltic Sea (Figure 4 – upper panel) from 1995 to
 260 2020. Waterborne inflows comprise the sum of river runoff and direct inflows, i.e. flows from
 261 point sources discharging directly into the Baltic Sea. These point sources are not included in
 262 our experimental setup or in the bias correction. However, their contribution to the total
 263 waterborne inflow to the Baltic Sea is only about 1% (HELCOM, 1998).



264



265

266 **Figure 4.** Selected HELCOM (upper panel) and OSPAR (lower panel) basins for which
 267 inflows are considered. For OSPAR, the Spanish Atlantic basin is limited to the coast
 268 of Northern Spain.

269 Under the umbrella of the OSPAR Convention (Convention for the Protection of the Marine
 270 Environment of the North-East Atlantic), the IGC-EMO (Intersessional Correspondence Group
 271 for Eutrophication Modelling) database (Lenhart et al., 2010) of daily riverine freshwater
 272 inflows and nutrient loads was compiled by Van Leeuwen and Lenhart (2021), covering the
 273 major rivers discharging into the Baltic Sea, the North Sea and the Northeast Atlantic. An
 274 updated database covering a total of 370 rivers was mapped onto the flow grid of the European
 275 1/12° domain of the HD model by Van Leeuwen and Hagemann (2023). The associated
 276 catchment areas of these rivers, which flow into a particular specific sea basin, do not cover the
 277 entire catchment area of the respective basin (see Table 1) so that the total inflow of the sea

278 basin is underrepresented by the IGC-EMO data. To generate basin-wide estimates, we have
 279 up-scaled these values by dividing the integrated IGC-EMO river discharges in a basin by the
 280 fractional coverage of the entire basin catchment on the HD grid. Basin estimates for which the
 281 fractional coverage is less than 75% are considered to be highly uncertain and are therefore
 282 provided for completeness only, but are not included in the assessment of simulated inflows.

283 **Table 1.** Sea basin catchment areas on the HD model grid and the fractional catchment
 284 coverage of the associated IGC-EMO rivers.

Sea basin	HD Area [km ²]		
	IGC-EMO	Total	Coverage
Baltic Sea	1513967	1671823	90.6%
Bothnian Bay	238898	258420	92.4%
Bothnian Sea	199908	219375	91.1%
Gulf of Finland	379628	412412	92.1%
Gulf of Riga	124386	134025	92.8%
Baltic Proper	494929	551295	89.8%
Danish Straits	6731	19417	34.7%
Kattegat	69487	76876	90.4%
Norwegian Barents Sea	0	81004	0.0%
Norwegian Sea	0	58408	0.0%
Skagerrak	89060	101787	87.5%
North Sea	514334	599755	85.8%
German Bight	201233	208807	96.4%
Norwegian North Sea	4590	31327	14.7%
English Channel	94327	122235	77.2%
Celtic Sea	41122	44845	91.7%
Irish Sea	29748	35584	83.6%
French Atlantic	207657	257981	80.5%
Northern Spanish Atlantic	17692	46574	38.0%

285

286 In addition, we used estimates of long-term mean sub-basin-wide inflows to the North Sea
 287 and Northeast Atlantic, published directly by OSPAR (Farkas and Skarbøvik, 2021). Figure 4
 288 (lower panel) shows the selected OSPAR basins for which the inflows are considered. It should
 289 be noted that the sea basin inflows provided by the different OSPAR countries are not
 290 consistent. Some countries include discharge estimates for unmonitored areas, while others do
 291 not (Table 2). In addition, the sea basin catchment coverage of the monitored areas varies
 292 between the countries. Note also that we have excluded the Spanish Atlantic from our
 293 comparisons for the following reason. Here, we limited the Spanish Atlantic basin to the coast
 294 of northern Spain (see Figure 4 – lower panel) to allow a comparison with the IGC-EMO data
 295 as the IGC-EMO data only cover rivers in this region, hereafter referred to as NSpA. These
 296 rivers cover about 38% of the total NSpA area on the HD model grid (Table 1), while the
 297 OSPAR data for NSpA cover about 50% (23201 km²; Farkas and Skarbøvik, 2021). However,
 298 the associated IGC-EMO discharge from 1961-1990 (629 m³/s) is 75 % larger than the OSPAR
 299 long-term mean average (359 m³/s). Therefore, both inflow values are unlikely to be
 300 representative for the NSpA region and this region is not considered in the following.

301

302 **Table 2.** Country catchment coverage of OSPAR data and inclusion of estimates for
 303 unmonitored areas (Borgvang et al., 2008). NI means that no information on the
 304 coverage was provided.

Country	Coverage	Unmonitored
Belgium	> 90%	No
Denmark	NI	Yes ³
France	84%	Yes
Germany	>90%	No ¹
Ireland	NI	Yes
Netherlands	>90%	No
Norway	ca. 50%	Yes
Portugal	NI	No
Spain	NI	No
Sweden	88.7%	Yes
United Kingdom	ca. 80% ²	No

305
 306
 307

¹ Only for Eider river

² 10% in direct discharge

³ e.g. Farkas and Skarbøvik (2021)

308 2.6 Ocean model experiments

309 To assess the effect of using bias corrected river discharge on simulated salinity in the German
 310 Bight, we used version 3.6 of the Nucleus for European Modelling of the Ocean (NEMO;
 311 Madec et al., 2017) and adopted a domain setup used by Ho-Hagemann et al. (2020). This
 312 domain covers the region of the north-west European shelf, the North Sea and the Baltic Sea
 313 between 19.89 E to 30.16 E and 40.07 N to 65.93 N with a resolution of two nautical miles (ca
 314 3.6 km). We used the atmospheric forcing from ERA5 and the ocean boundary forcing from
 315 the ECMWF Ocean Reanalysis System 5 (ORAS5; Zuo et al., 2019) to conduct two simulations
 316 from 2010 to 2018. Initial conditions were taken from a 20-years spin-up simulation driven by
 317 ERA5 data, so that the deeper ocean layers could adapt to the present-day climate (S. Grayek,
 318 pers. comm., 2023). Note that for the evaluation of results, we neglected the year 2010 to have
 319 an additional spin-up where NEMO could adapt to the specific transient conditions within each
 320 of the two experiments. For the German Bight, this spin-up of one year is sufficient as the
 321 residence time of water may comprise only up to four months (Becker et al., 1999). In these
 322 two simulationsexperiments, the daily riverine inflow into the ocean was taken from the
 323 uncorrected and bias corrected discharges of HD5-WFDE5HDW, which were converted to the
 324 NEMO grid using a procedure of Nguyen et al. (2024). For each HD model river mouth box,
 325 we associated the nearest coastal ocean box on the NEMO grid if such a box was found within
 326 a search radius of 200 km. Such a large radius is necessary because the NEMO coastline is very
 327 smooth, so many estuaries and bays in the HD model grid are not resolved by NEMO. If no
 328 ocean box was found, the corresponding HD model box was not linked. Consequently, the
 329 simulated discharge data at the river mouths were placed as freshwater inflow into the
 330 corresponding NEMO grid boxes.

331 2.7 Evaluation metrics

332 The evaluation of the simulated discharge was performed for the grid boxes corresponding to
333 the discharge station locations within the river network. For the evaluation at these station
334 locations, we used the mean bias, the Pearson correlation coefficient and the Kling-Gupta
335 efficiency (KGE; Gupta et al., 2009; Kling et al., 2012). ~~Both-All~~ metrics were calculated with
336 simulated and observed daily discharge time series for the period considered, using only those
337 days for which observed data are available. The KGE is a quality metric combining bias,
338 correlation and coefficient of variation. If a simulated discharge time series has a KGE > -0.41,
339 then it is a better representation of the observations than the use of the observed long-term mean
340 discharge (Knoben et al., 2019). Note that many ocean model applications still use the latter
341 method.

342 For the evaluation of simulated salinity in the NEMO experiments, we used daily values and
343 considered

- 344 • the mean bias
- 345 • the correlation of simulated and observed time series expressed by the Pearson
346 correlation coefficient
- 347 • the variability ratio defined by the ratio of the simulated and observed coefficients of
348 variation
- 349 • the normalized root-mean-square-error (RSME)
- 350 • the centered RSME.

351 The first four metrics are described, e.g., in Hagemann et al. (2020), while the centered RSME
352 is described, e.g., in Taylor (2001).

353 **3 Evaluation of the bias correction**

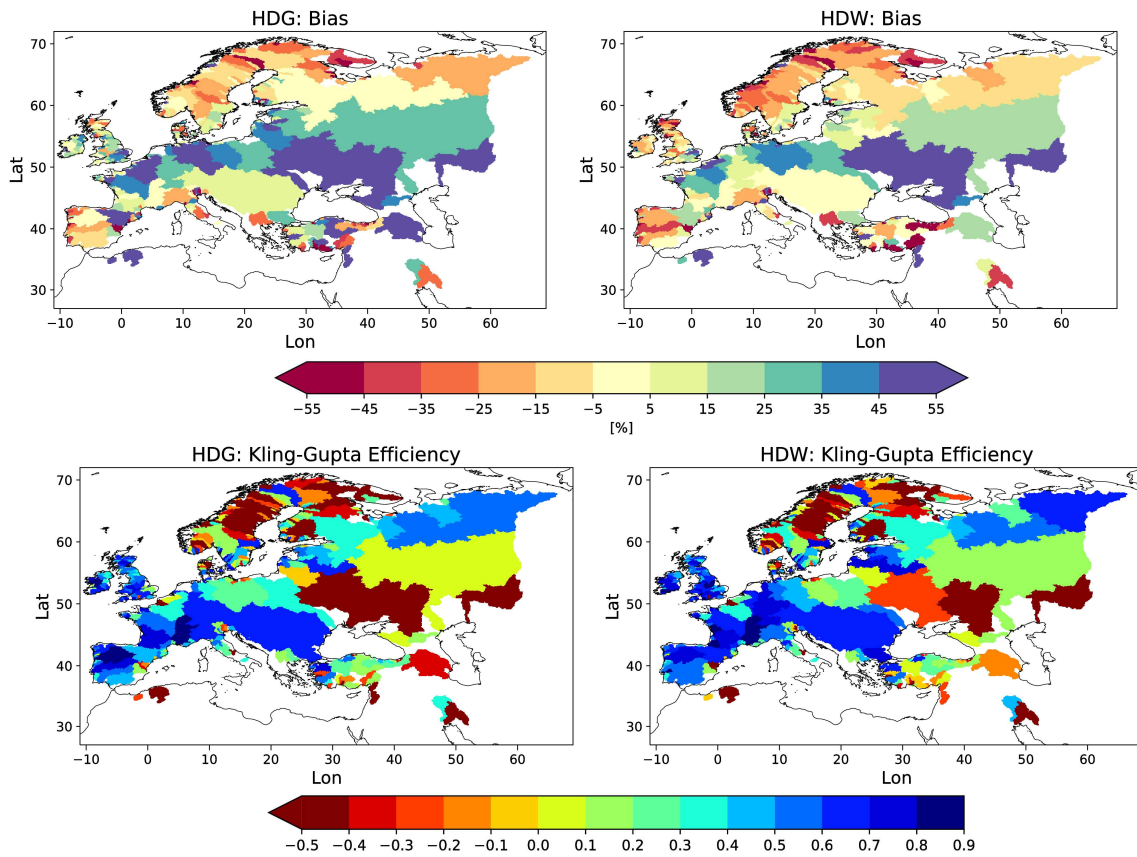
354 Below, various metrics have been calculated at the station locations and at the river mouths.
355 However, these measures have been assigned to the respective catchment areas for the purpose
356 of graphical presentation.

357 **3.1 Evaluation of simulated discharge**

358 The distribution of bias and KGE for HD5-GSWP3HDG and HD5-WFDE5HDW during 1979-
359 2014 (Figure 5) is quite similar to the pattern shown by Hagemann and Stacke (2022) for the
360 ERA5-based discharge. For both simulations, the general discharge behaviour is well captured
361 (KGE > 0.4) for many European rivers, especially in Northern Iberia, Western and Central
362 Europe, and over Northern Russia (Figure 5, lower row). As expected (cf. Hagemann et al.,
363 2020), larger deviations of the simulated from observed discharges occur for rivers that are
364 heavily influenced by human activities such as water abstraction, e.g. for irrigation, and
365 regulation, e.g. by dams. This is the case for many Scandinavian and Turkish rivers as well as
366 the Volga and Don.

367 In general, the HD5-WFDE5HDW discharges are slightly drier than the HD5-GSWP3HDG
368 discharges, as indicated by larger dry biases in Northern Europe and smaller wet biases in
369 Central Europe. Despite the differences in bias distribution, the KGEs of HD5-WFDE5HDW
370 are similar to or slightly better than those of HD5-GSWP3HDG. Compared to the ERA5-based
371 discharge of Hagemann and Stacke (2022), HD5-WFDE5HDW tends to have smaller discharge
372 biases and better KGEs. This is an expected behaviour caused by the application of a bias
373 correction methodology to the ERA5 data in the generation of the WFDE5 data (cf. Sect. 2.1).
374 An exception to this general improvement occurs over Northern Europe, where the dry bias of
375 HD5-WFDE5HDW tends to be slightly larger and the KGEs lower. Note that Hagemann and

376 Stacke (2022) attributed the dry bias over Northern Europe to an overestimation of the
 377 evapotranspiration simulated by HydroPy.



382 **Figure 5.** Mean discharge bias [%] (upper row) and Kling-Gupta-efficienciesKGE (lower
 383 row) for HD5-GSWP3HDG (left) and HD5-WFDE5HDW (right) during 1979-2014.

384 In order to analyse how much the bias correction affects the daily sequence of river runoff
 385 at the station locations, we calculated the correlation between the simulated discharges and the
 386 observations. Supplementary Figure S1 shows that the correlation patterns of HDW and HDW-
 387 BC with observed discharges are quite similar. For rivers where differences can be identified,
 388 the correlation mostly increases for HDW-BC. The correlation between HDW and HDW-BC
 389 is generally higher than 0.95, and only a very few rivers show correlations lower than 0.9. These
 390 rivers are usually rivers that are heavily influenced by human activities, such as the Volga and
 391 the Luleaelven.

392 **3.2 Added value of the three-part-quantile bias correction**

393 In this section, we consider the effect of the bias correction at the station locations and
 394 investigate whether the three-part-quantile bias correction adds value compared to using only
 395 the mean bias correction. For this purpose, we use HD5-WFDE5HDW and the period 1979-
 396 2014.

397 Both bias correction methods reduce the mean discharge bias to zero or close to zero in the
 398 case of the three-part-quantile bias correction due to the smoothing around the percentile range
 399 thresholds (see Table 3 for selected rivers). When the mean bias correction is applied, the KGEs
 400 (Figure 6 – left panel) are noticeably improved over Western and Central Europe. However,

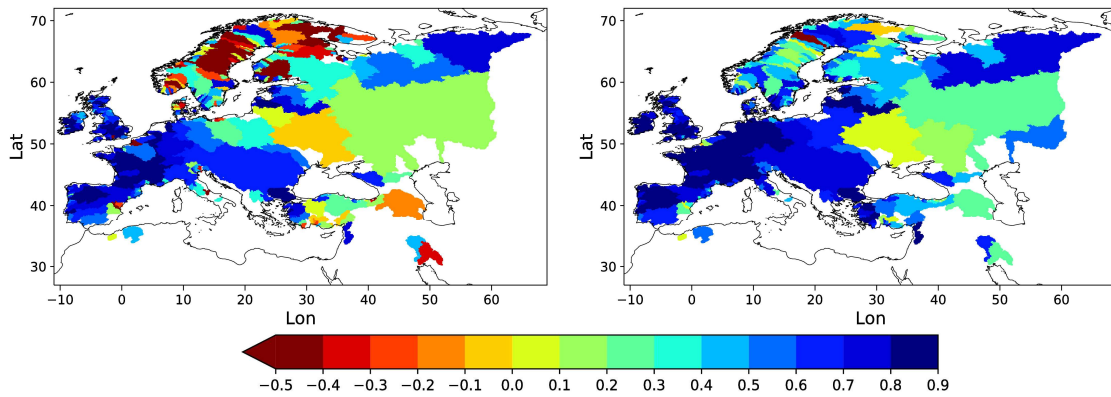
401 with a few exceptions, the KGE pattern over Northern Europe and other areas remains largely
 402 unchanged. This indicates that a correction of the long-term bias in the annual mean discharge
 403 over these areas is not sufficient. Only with the three-part-quantile bias correction does the KGE
 404 (Figure 6 – right panel, Table 3 for selected rivers) improve considerably over these areas, with
 405 the largest improvements occurring over Scandinavia. The three-part-quantile bias correction
 406 also leads to some further improvements over Western and Central Europe, where the bias
 407 corrected discharge with the mean bias correction already shows relatively high KGE values,
 408 e.g. for the rivers Elbe, Rhine and Weser.

409 **Table 3.** Mean bias and KGE of simulated (HD5-WFDE5HDW) and bias corrected
 410 discharge for selected rivers during 1979-2014 for selected rivers, where the three-
 411 quantile bias correction led to a noticeable KGE improvement in comparison to the
 412 mean bias correction.

River	HD5-WFDE5		Mean Bias corr.		3-quantile Bias corr.	
	Bias	KGE	Bias	KGE	Bias	KGE
Dalaelven	-32.02 %	-0.32	0 %	-0.28	0.01 %	0.48
Elbe	36.44 %	0.46	0 %	0.60	-0.06 %	0.85
Indalsaelven	-19.32 %	-0.79	0 %	-0.78	-0.02 %	0.38
Odra	41.30 %	0.14	0 %	0.25	0.01 %	0.75
Rhine	14.60 %	0.74	0 %	0.78	-0.02 %	0.85
Weser	33.15 %	0.55	0 %	0.70	-0.01 %	0.90

413

414

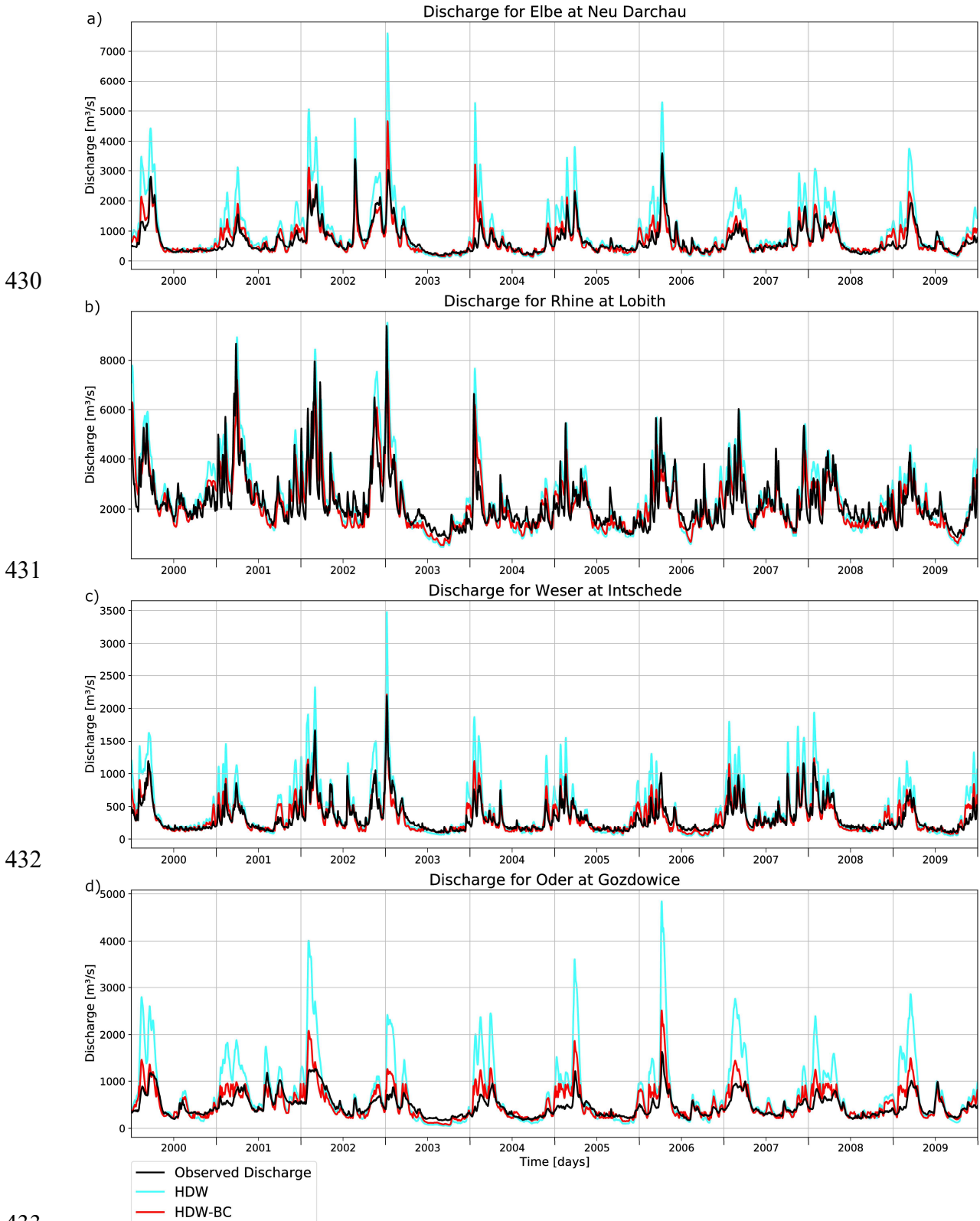


415

416

417 **Figure 6.** Kling-Gupta efficiencies KGE for bias corrected HDW5-WFDE5 discharges
 418 using the mean bias correction (left) and the three-part-quantile bias correction (right)
 419 during 1979-2014.

420 To visualise the effect of the three-part-quantile bias correction on the simulated daily
 421 discharges, we consider the corresponding discharge curves for the period 2000-2009 for
 422 selected large rivers. The respective biases and KGE are shown in Table 3 for the period 1979-
 423 2014. For the rivers, Elbe, Weser and Oder, the peak discharges are generally overestimated,
 424 while the low flows are close to the observed values (Figure 7a,c,d). The correction of the high
 425 percentiles leads to a considerable improvement in the representation of the peak discharges,
 426 while the change in the low flows is rather small. The discharge of the Rhine (Figure 7b) is well
 427 represented by HD5-WFDE5HDW. However, the small downward correction of the peak
 428 discharges and the slight increase in the low flows still lead to an improved discharge curve,
 429 which is also indicated by the increased KGE (Table 3).

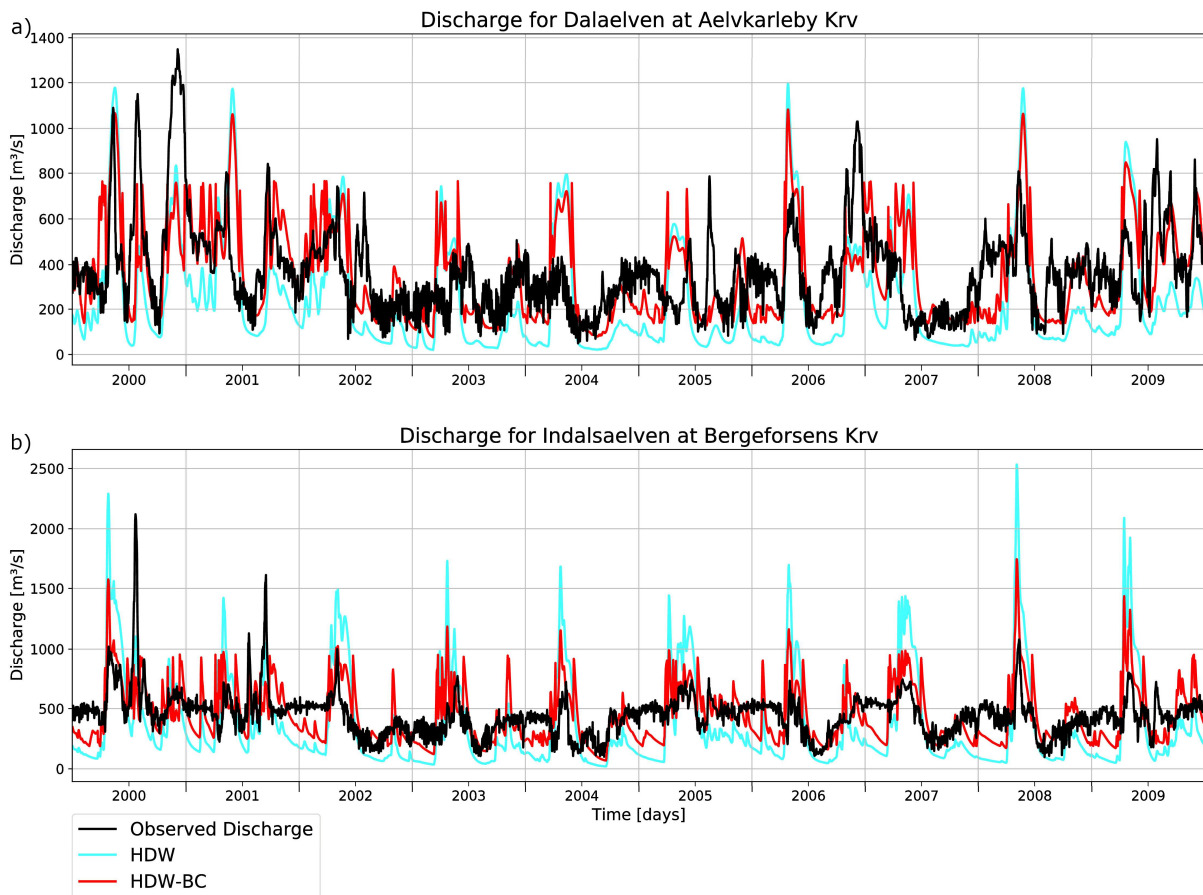


434 **Figure 7.** Observed and simulated daily discharges for the rivers a) Elbe, b) (1st panel);
 435 Rhine, c) (2nd panel); Weser c) (3rd panel) and d) Odra d) (4th panel) during 2000-2009.

436 As mentioned above, the greatest improvements from the three-part-quantile bias correction
 437 compared to the application of the mean bias correction occur over Scandinavia. Here many

438 rivers are highly regulated. For this reason, the discharge curves of the Daleaelven and
 439 Indalsaelven rivers are examined in more detail in Figure 8. The observed discharges clearly
 440 show the effect of the human regulation, where regulation leads to the elimination of peak
 441 discharges, while maintaining certain flows during low flow periods. Figure 8 shows that, on
 442 the one hand, peak discharges are often suppressed or reduced, especially during the spring,
 443 and that, on the other hand, low-flow periods are either almost absent (especially for the
 444 Indalsaelven) or show a rather noisy, unnatural daily variability. Here, the bias correction
 445 partially mimics these regulation effects by reducing the peak discharges and increasing the low
 446 flows.

447



448

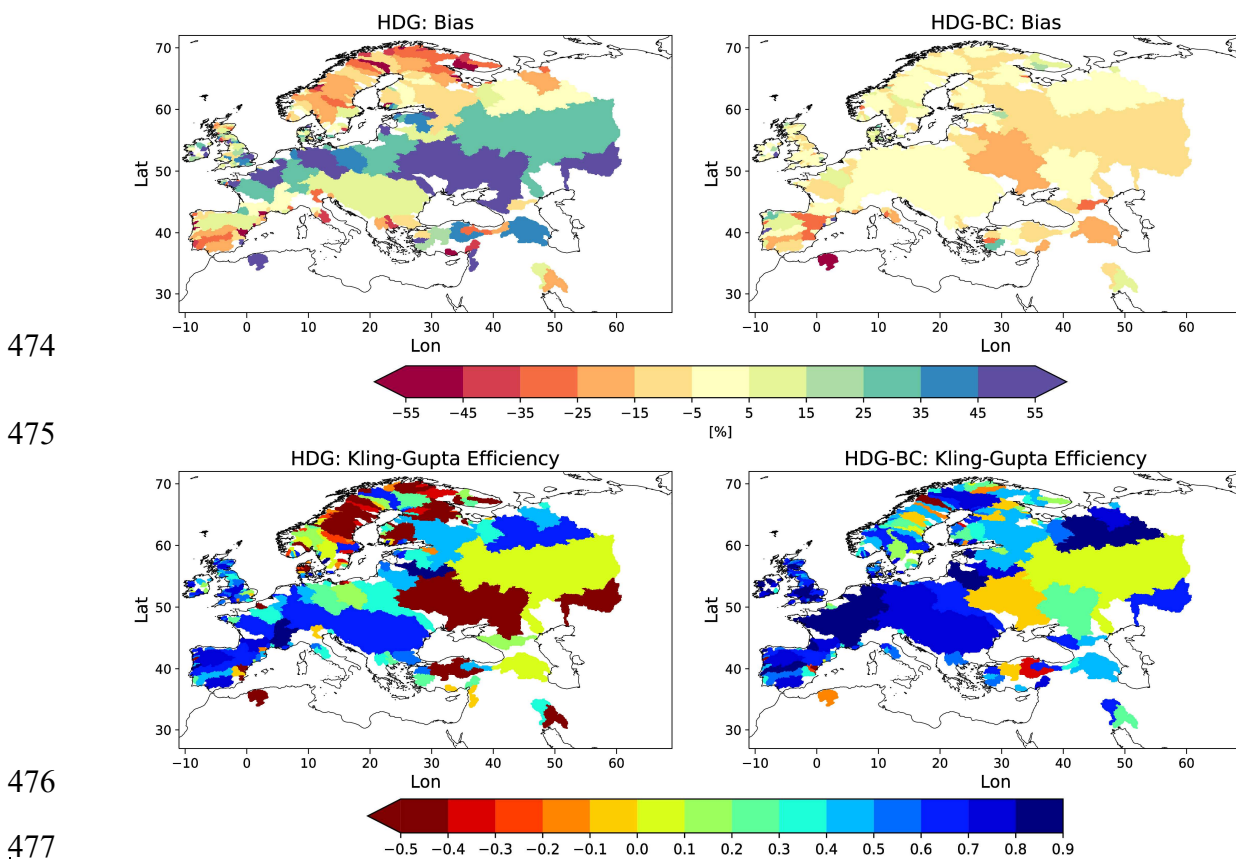
449 **Figure 8.** Observed and simulated daily discharges for the rivers **a)** Daleaelven (**1st panel**)
 450 and **b)** Indalsaelven (**2nd panel**) during 2000-2009.

451 3.3 Application of the bias correction for a different time period

452 To consider the effect of the bias correction for the applications over different time periods, we
 453 derived bias correction factors for HDG5-GSWP3 during 1979-2014 and applied the factors for
 454 the period 1950-1978.

455 For HD5-GSWP3G, the distributions of bias and ~~Kling-Gupta efficiencies~~ KGE are quite
 456 similar between the two periods 1950-1978 (Figure 9 – left column) and 1979-2014 (Figure 5
 457 – left column). Consequently, the bias correction leads to similar improvements in the KGE
 458 (Figure 9) as for the most recent period (not shown). The bias also becomes small for most of
 459 the rivers. Noticeable exceptions are the Dnjepr, Volga and some rivers in Southern Europe.

460 This may be related to differences in the anthropogenic influence on the discharge between the
 461 two periods, as is the case for the river Ebro. Here, the large wet bias (51.65 %) in the more
 462 recent period is contrasted with a small wet bias (12.05%) in the earlier period (Figure 10).
 463 Since large anthropogenic water abstractions occur in the Ebro River (Merchán et al., 2013),
 464 this seems to be related to the different irrigation activities in the two periods, which are much
 465 more pronounced in the more recent years. The latter can be seen by looking at the observed
 466 daily discharges between 1960-1969 and 2000-2009 (Figure 10). In the earlier period, the Ebro
 467 discharge still shows some variations according to the sequence of weather events in the dry
 468 season. However, in the later period, the observed discharge includes only very small variations
 469 during the dry season, indicating more intense human water abstraction than in the earlier
 470 period. Consequently, the bias correction based on the recent wet bias leads to a dry bias (-
 471 25.78 %) in the corrected Ebro discharge in the earlier period. However, the KGE decreases
 472 only slightly from 0.68 to 0.63, so that the deterioration of the mean bias seems to be largely
 473 compensated by the correction of the different percentile ranges.



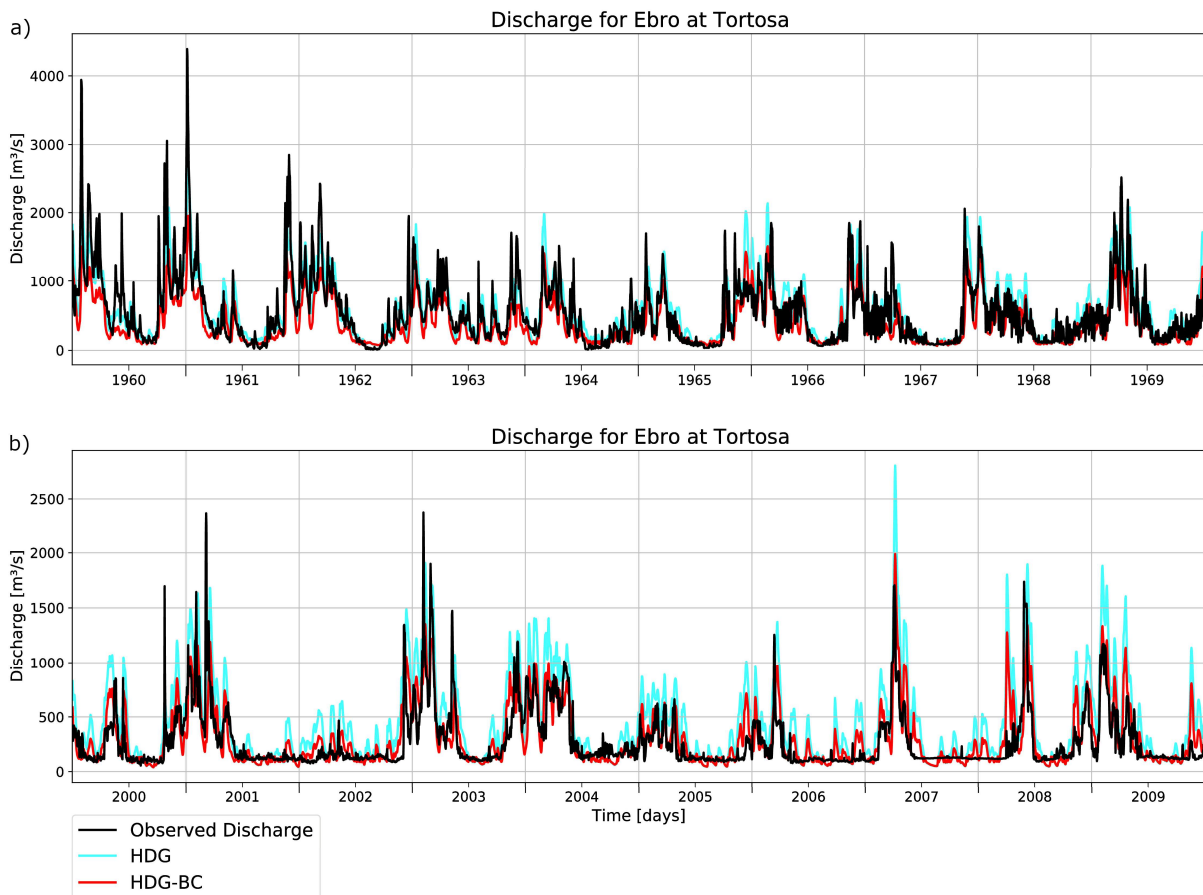
478 **Figure 9.** Mean discharge bias [%] (upper row) and Kling-Gupta efficienciesKGE (lower
 479 row) for HDG5-GSWP3G (left) and bias-correctedHDG5-GSWP3_BC data (right)
 480 during 1950-1978.

481 3.4 Effect of the bias correction on contemporary trends

482 As mentioned in Sect. 2.4, our three-quantile bias correction is similar to a very coarse quantile
 483 mapping, and quantile mapping has been flagged as potentially not suitable for climate
 484 simulations as it has been shown to modify trends (e.g. references in (e.g. references in Cannon
 485 et al., 2015). However, Maraun et al. (2017) pointed out that a debate has arisen about whether
 486 trend modification by variance-adjusting bias correction methods actually improves or degrades

487 the raw climate change signal. They further argued that purely statistical arguments cannot
488 resolve this issue, which requires process understanding. With respect to runoff, the latter needs
489 to take into account spatial and temporal characteristics of rivers and events, which is beyond
490 the scope of the present large-scale study.

491



492

493 **Figure 9.** **Figure 10.** Observed and simulated daily discharge based on HDG of HD5-
494 GSWP3 for the Ebro river during a) 1960-1969 (1st panel) and b) 2000-2009 (2nd
495 panel).

496 To investigate the effect of the bias correction on contemporary trends, we calculated trends in
497 the annual maximum, mean and minimum discharge for the period 1979-2014 and compared
498 the results for HDW and HDW-BC (Figure 11). The trend patterns are generally within the
499 range spanned by the two datasets considered in Hagemann and Stacke (2022). For the annual
500 maximum and mean discharge, the trend patterns are only slightly changed by the bias
501 correction. For the annual minimum discharge, the trend pattern is quite similar in HDW and
502 HDW-BC. However, there are a few more rivers where the magnitude of the trend is affected
503 by the bias correction. This is particularly the case over Scandinavia where many rivers are
504 regulated, so that that the correction of the low percentile range is often strong to account for
505 the effect of regulation on low flows (cf. Sect. 3.2).

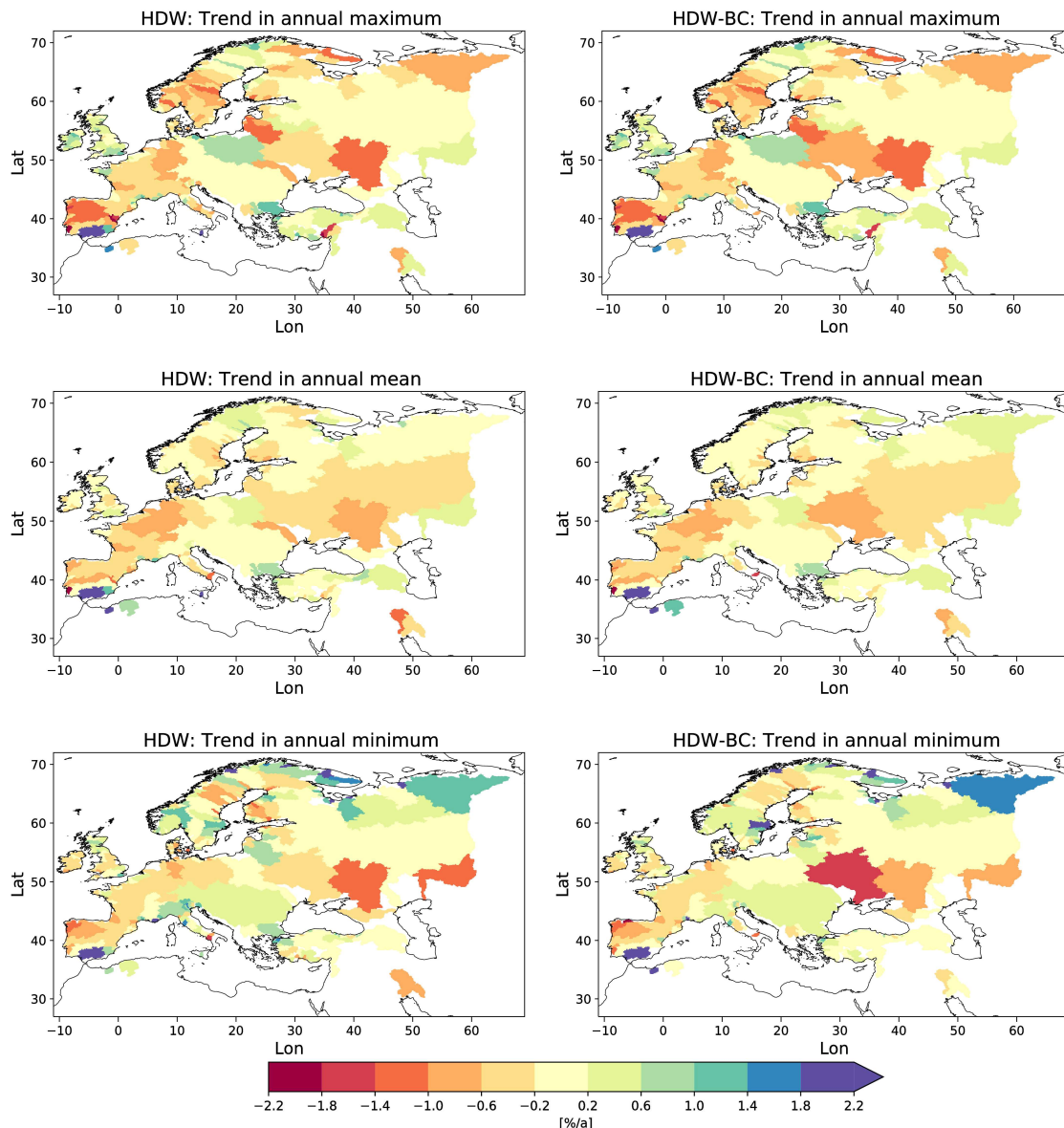


Figure 10. Trends in annual maximum (1st row), mean (2nd row) and minimum (3rd row) discharge [%/a] for HDW (left column) and HDW-BC (right column) from 1979-2014.

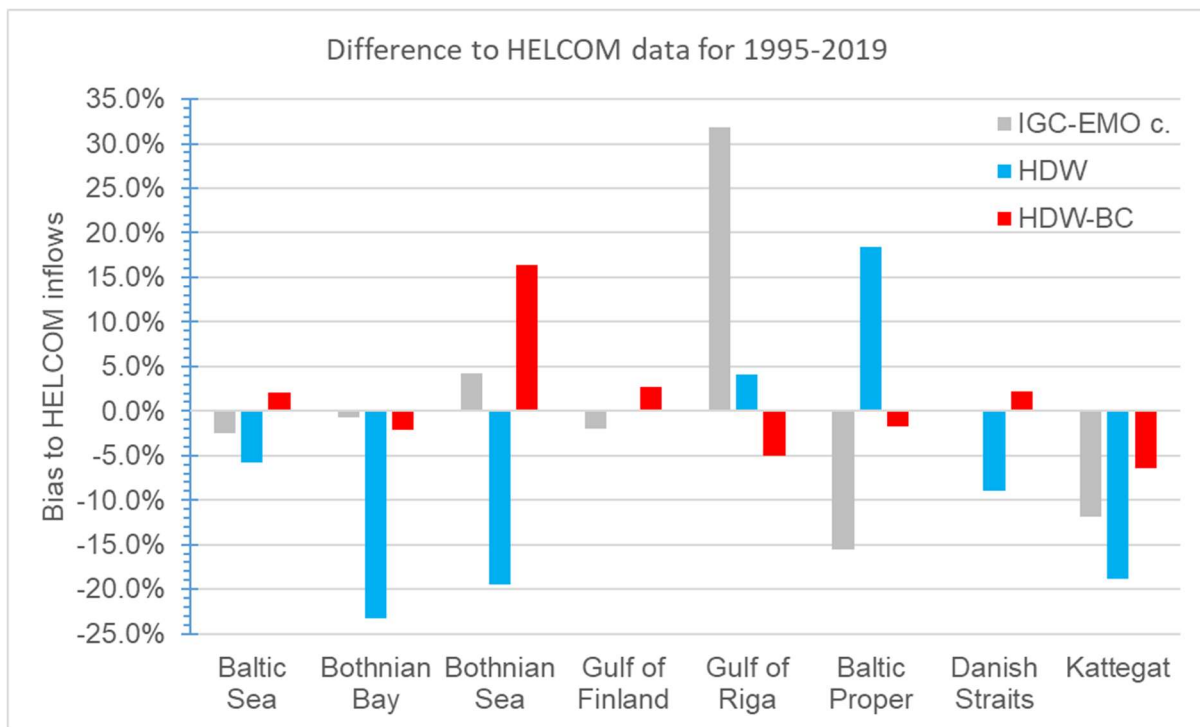
4 Evaluation of the inflow into sea basins

To evaluate the simulated and bias corrected discharges at the river mouths, we considered the integrated inflow into different sea basins. First, we evaluated the discharges into the Baltic Sea using HELCOM and IGC-EMO data in Section 4.1. We then compared the discharges to the North Sea and the Northeast Atlantic with OSPAR and up-scaled (see Section 2.5) IGC-EMO data in Section 4.2.

4.1 Baltic Sea

In order to achieve a maximum overlap of the simulated discharge time series data with the HELCOM data (cf. Section 2.5), we considered 1995-2019 as the evaluation period for the Baltic Sea and its seven sub-basins (Figure 4 – upper panel). For the whole Baltic Sea and most of its sub-basins, the bias correction improves the basin inflows if compared to the HELCOM

526 estimates (Table 4, Figure 12). Only for the Gulf of Finland and the Gulf of Riga, the bias
 527 correction leads to a slightly larger bias while the biases of ~~HD5-WFDE5~~~~HDW~~ in these basins
 528 are relatively small. When the simulated inflows are compared with the IGC-EMO estimates,
 529 similar results are obtained, except for the Gulf of Riga. Here, the IGC-EMO estimates are
 530 about 32% larger than the HELCOM estimates, indicating a larger uncertainty in at least one of
 531 these two estimates. For the Gulf of Riga basin, the major part of the inflow is contributed by
 532 the Daugava river. In IGC-EMO, the discharge from the Daugava is based on observed time
 533 series from 1970-1990. These data were extended to earlier and later periods, e.g. by
 534 climatological values and trend preservation (Van Leeuwen and Hagemann, 2023). For 1970-
 535 1990, the mean IGC-EMO discharge comprises 623 m³/s at the Daugava mouth, while this has
 536 increased by ca. 45% in 1995-2019 (902 m³/s). However, this strong increase cannot be seen in
 537 the observed discharge time series at the station Daugavpils that covers about three quarter of
 538 the Daugava catchment. Here, the discharge increases only slightly from 1970-1999 (439 m³/s;
 539 95% temporal data coverage) to 1995-2019 (452 m³/s; 83% temporal data coverage). This
 540 indicates a large overestimation of the IGC-EMO Daugava discharge during 1995-2019 and,
 541 hence, also of the respective Gulf of Riga inflow.



542

543 **Figure 11. Figure 12.** Relative difference in basin inflows compared to HELCOM data
 544 for 1995-2019. Note that no IGC-EMO estimate is provided for the Danish Straits as
 545 the respective river catchment coverage in IGC-EMO is too small.

546 **Table 4.** Estimated and simulated inflows (unit: m³/s) into the Baltic Sea and its major
 547 sub-basins during 1995-2019. Note that for the Danish Straits no IGC-EMO estimate is
 548 provided as the respective catchment area coverage of the rivers in IGC-EMO is too low.

Sea basin	HELCOM	IGC-EMO c.	HD5-WFDE5 HDW	HDW-BC5 Bias-C.
Baltic Sea	15676	15286	14764	15995
Bothnian Bay	3444	3420	2642	3369

Bothnian Sea	2913	3038	2347	3391
Gulf of Finland	3519	3448	3520	3612
Gulf of Riga	1071	1411	1114	1017
Baltic Proper	3436	2901	4070	3377
Danish Straits	217	0	198	222
Kattegat	1077	949	873	1008

549

550 **4.2 North Sea and Northeast Atlantic**

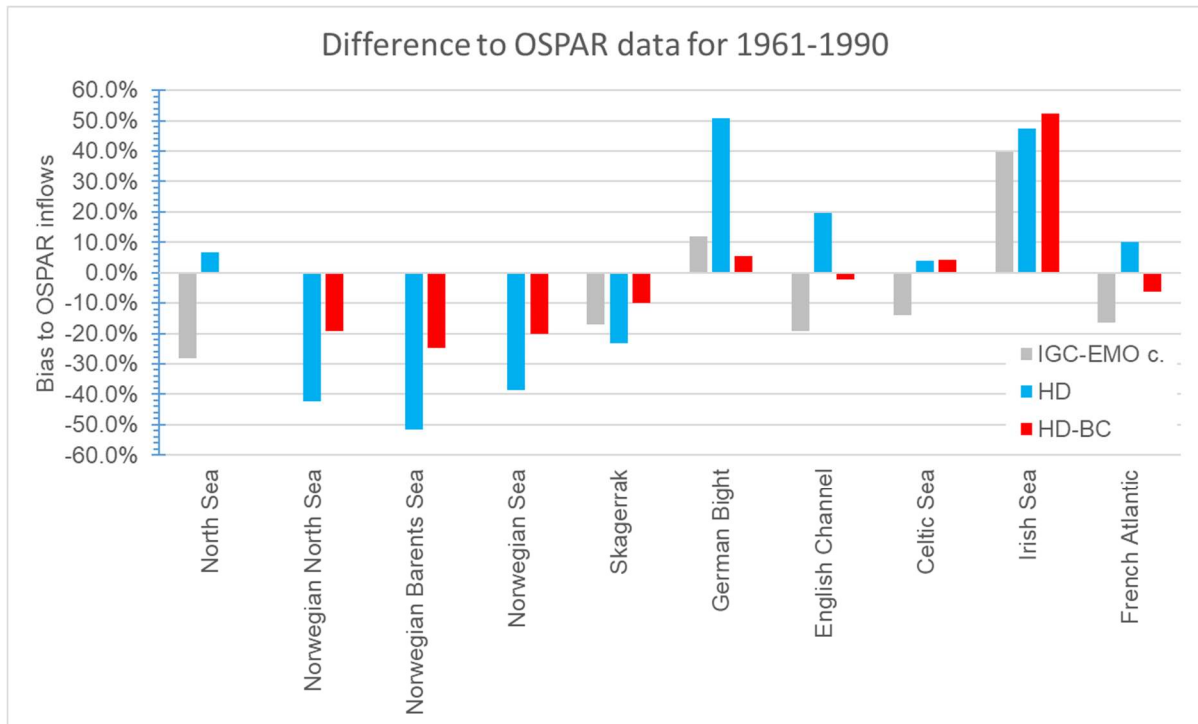
551 Due to the different treatment of unmonitored regions by the OSPAR countries (cf. Section
552 2.5), and thus of the respective sea basin areas, we have not corrected the OSPAR inflows.
553 Instead, we have also considered up-scaled IGC-EMO data as alternative estimates of basin
554 inflow (as in Section 4.1). Table 5 shows simulated and estimated basin inflows for the
555 considered OSPAR regions (cf. Figure 4 – lower panel). Note that IGC-EMO data for the
556 Norwegian shares of the Barents Sea, Norwegian Sea and North Sea, and the North Spanish
557 Atlantic are not included in the following comparisons due to their limited area coverage. When
558 comparing the simulated sea basin inflows with the OSPAR and IGC-EMO data, we found that
559 the bias correction improves the simulated inflows for most of the OSPAR regions (Figure 13).
560 Exceptions are the values for the Celtic Sea and the Irish Sea. For the Celtic Sea, the bias
561 corrected inflows are very close to the uncorrected inflows and the difference to the OSPAR
562 data is rather small. For the Irish Sea, the bias corrected inflows are somewhat larger than the
563 uncorrected ones, with both showing large differences (52.5% and 47.5%) to the OSPAR data.
564 Here both inflows are closer to the IGC-EMO estimate, which exceeds the OSPAR estimate by
565 about 40%.

566 **Table 5.** Estimated and simulated inflows (unit: m³/s) into major sub-basins of the North
567 Sea and the Northwest Atlantic during 1961-1990. Note that the North Sea does not
568 comprise Skagerrak and the English Channel. Up-scaled IGC-EMO basin estimates
569 for which the fractional catchment area-coverage (see Table 1) of IGC-EMO rivers is
570 less than 75% are considered as highly uncertain and are therefore only given in
571 brackets (cf. Sect. 2.5). The same applies to the OSPAR inflow into the Northern
572 Spanish Atlantic.

Sea basin	OSPAR	IGC-EMO c.	HD5- WFDE5HD	HD5-BiasC- BC
North Sea	9190	6600	9798	9164
Norwegian North Sea	3534	(1499)	2038	2856
Norwegian Barents Sea	2294	-	1106	1723
Norwegian Sea	3663	-	2242	2922
Skagerrak	2544	2113	1956	2292
German Bight	1344	1505	2025	1419
English Channel	1250	1011	1498	1222
Celtic Sea	976	839	1016	1016
Irish Sea	672	939	992	1025
French Atlantic	2862	2391	3147	2684
Northern Spanish Atlantic	(359)	(1655)	1104	1550

573

574 While the OSPAR values from Ireland include estimates for unmonitored areas, this is not
 575 the case for the United Kingdom (Table 2). Farkas and Skarbøvik (2021) list the rivers
 576 contributing to the OSPAR value (560 m³/s) from the United Kingdom part of the Irish Sea
 577 catchment (35000 km²). Adding up the catchment areas of each river, obtained from various
 578 online resources, gives a coverage of about 70%. In order to account for this under-
 579 representation of the catchment area, an up-scaling can be performed, similar to the treatment
 580 of the IGC-EMO data. This would give an estimate of about 803 m³/s for the UK-Irish Sea
 581 inflow from the United Kingdom and thus 915 m³/s for the whole Irish Sea. The respective
 582 IGC-EMO inflow is close to this value (+2.6%) and the overestimation of inflows is less
 583 pronounced for HD-~~WFDE5~~ and bias corrected discharges with +8.4% and +12% respectively.



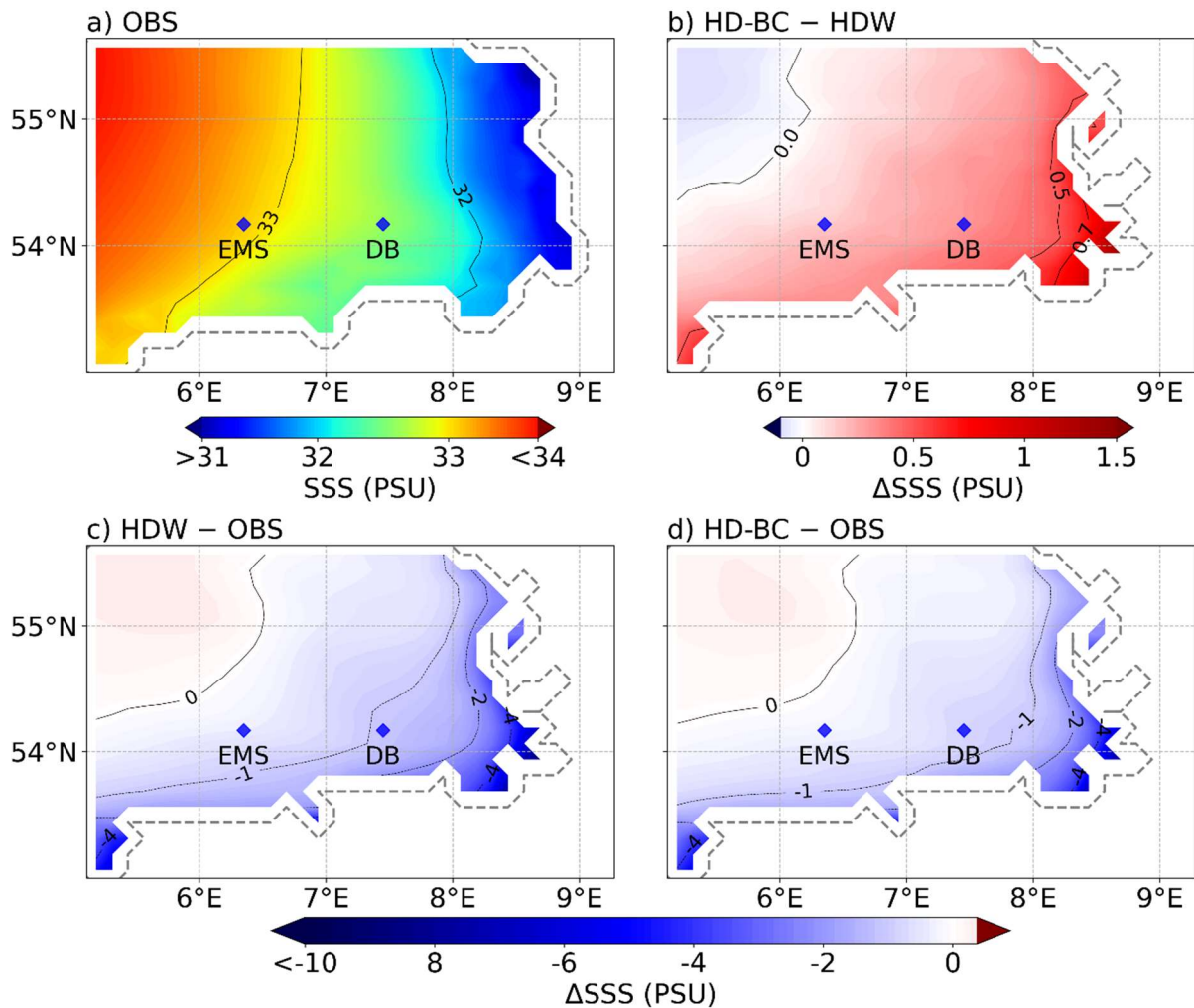
584
 585 **Figure 12. Figure 13.** Relative difference in basin inflows compared to OSPAR data
 586 for 1961-1990. IGC-EMO basin estimates for which the fractional area-catchment
 587 coverage (see Table 1) is less than 75% are not shown.

588 4.3 Simulated salinity in the German Bight

589 Using the two experiments described in Sect. 2.6, we evaluated the simulated sea surface
 590 salinity (SSS) with satellite-based analyses and in-situ observations for the period 2010 to 2018.
 591 The SSS analyses were derived using a multivariate optimal interpolation algorithm that
 592 combines sea surface salinity images from several satellite sources, such as the National
 593 Aeronautics and Space Administration (~~NASA~~) Soil Moisture Active Passive (~~SMAP~~) satellite
 594 and the European Space Agency (~~ESA~~) Soil Moisture Ocean Salinity (~~SMOS~~) satellite, with
 595 in-situ salinity measurements (Droghei et al., 2018). These SSS data are available with a spatial
 596 resolution of 0.125°.

597 Figure 14a shows the mean analysed SSS in the German Bight for the period 2010-2018,
 598 with lower salinities near the west coast of Germany and higher salinities towards the west. The
 599 NEMO simulation using the uncorrected discharges of ~~HD5-WFDE5~~HDW (Figure 14c) has

600 too low SSS in coastal areas, especially near the estuaries. This low bias is reduced using the
 601 bias corrected discharges (Figure 14d), as the general effect of the bias correction in the German
 602 Bight leads to reduced riverine inflows (cf. Figure 13) and hence increased SSS in coastal areas
 603 (Figure 14b). Similar improvements can also be seen in June 2013 when the Elbe flood is
 604 strongly influences the SSS of the German Bight (Figure S2). Here, the increase in salinity due
 605 to the bias corrected runoff (Figure S2b) is more pronounced than in the long-term mean (Figure
 606 14b). In addition, we found that use of the bias corrected river runoff also improves the SSS
 607 variability expressed by its coefficient of variation, shown in Figure 15.



608

609 **Figure 13-14.** Mean analyzed SSS: a) Droghei et al. (2018) data (OBS) and
 610 various SSS differences of the NEMO experiments in the German Bight for the period
 611 from 2010 to 2018. The SSS differences comprise b) HD-BC5-Bias-C. minus HD5-
 612 WFDE5HDW, c) HD5-WFDE5HDW minus OBS, and d) HD-BC5-Bias-C. minus
 613 OBS.

614

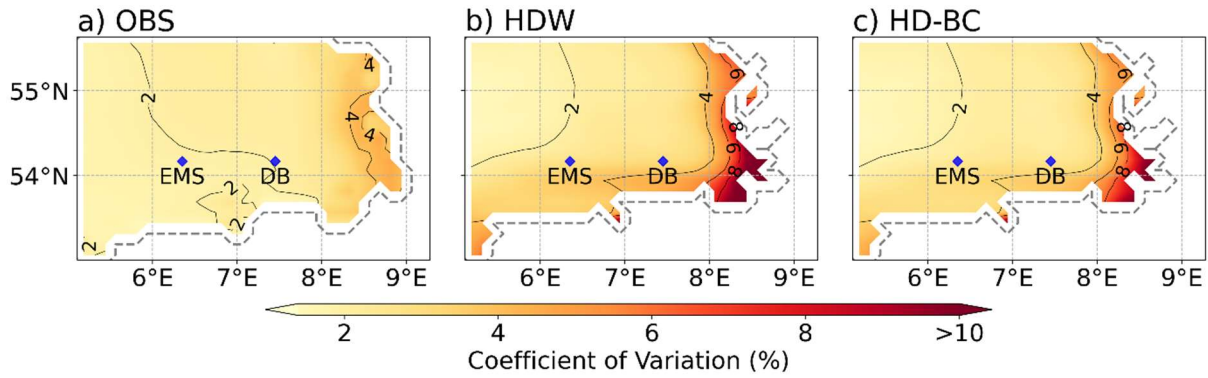


Figure 15. Coefficients of variation of SSS in the German Bight for the period from 2011-2018: a) OBS, b) HDW and c) HD-BC

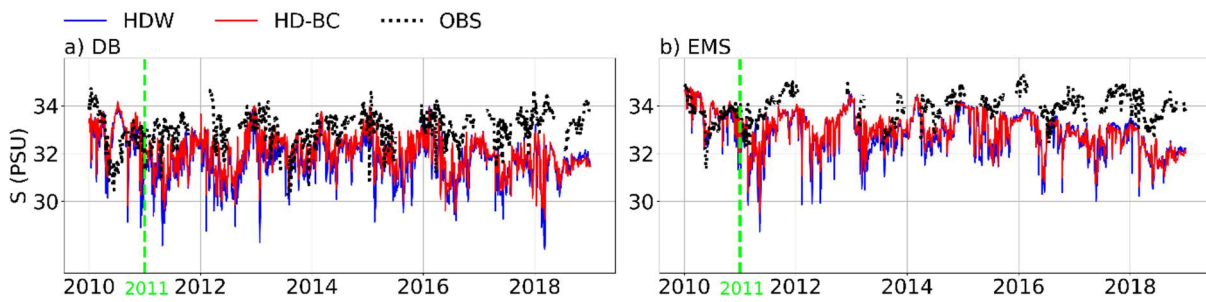


Figure 16. Observed (OBS) and simulated daily time series of salinity in 6 m depth for the MARNET stations: a) *Deutsche Bucht* (DB) and b) *EMS*. Unit: PSU. The blue and red solid lines correspond to the HDW and HD-BC experiments, respectively. The green line separates the spin-up period in 2010 from the evaluation period 2011-2018.

In addition, we had access to salinity measurements at three-two stations in the German Bight operated by the German Federal Maritime and Hydrographic Agency BSH as part of the Marine Environmental Monitoring Network in the North and Baltic Seas (MARNET). These three-two stations are Deutsche Bucht (DB; located at 54.17°N, 7.45°E) and, EMS (54.17°N, 6.35°E) and Nordsee-Boje II (NSB; 55°N, 6.33°E) and their locations are shown in Figure 14. In general, the bias corrected discharges lead to improved characteristics of the daily salinity at 6 m depth at the Deutsche Bucht and EMS stations (Figure 16, Table 6). Here the bias, normalized and centred RSME are decreased, and the coefficient of variation is closer to the salinity observations for HDW-BC. This means that the bias correction improves the mean and the variability of the simulated salinity at these stations. However, the correlation with the observed salinity measurements is somewhat reduced. Note that temporal SSS variations are strongly influenced by local currents, vertical mixing and wind-wave-surface interactions. Therefore, signals from an improved river runoff can easily be obscured by the noise from these processes, which can also differ at the point scale of the station measurements and at the grid scale of the respective NEMO grid box. This is reflected in the relatively low correlation values. Furthermore, this can be seen when the gridded SSS data of Droghei et al. (2018) are used as a reference for the metrics at the station locations (Supplementary Table S1). Here, all metrics improve with HDW-BC, even the correlation. However, the correlation is lower than with the station observations, which is also the case for the correlation of the gridded SSS data itself with the station observations (*Deutsche Bucht*: 0.15; *EMS*: 0.18). Considering only the year

2013, when the influence of the Elbe flood on the salinity at the *Deutsche Bucht* station is more pronounced (Nguyen et al., 2024), the correlation also improves when using HDW-BC for both references (Table 6 and S1). an improved simulation of the daily salinity at 6 m depth at the stations DB and EMS. Here the RSME decreases from 1.70 to 1.45 and from 1.43 to 1.32, respectively. It seems that in NEMO the positive effect of using bias corrected discharges is limited to near-surface salinities, as there is no noticeable effect at 30 m depth (not shown). This is consistent with the fact that the *Deutsche Bucht* and *EMS* stations are located in an area where the salinity is temporarily stratified, depending on the meteorological conditions and the intensity of river runoff (Klein and Frohse, 2008). NSB is not considered in detail as it is located further offshore where no noticeable SSS changes were introduced by using bias corrected discharges (Figure 13b).

In summary, the results of the NEMO experiments indicate the beneficial effect of using bias corrected discharges on the simulated SSS in coastal areas. However, although the low SSS biases are reduced by using the bias corrected discharges, the simulated SSS is still underestimated in coastal areas, especially close to the estuaries of large rivers (Figure 14d). This may be attributed to the rather smooth coastline of the NEMO ocean grid. Here, most parts of the large estuaries of the rivers Elbe, Ems and Weser are not included. In reality, a major part of the mixing of the riverine freshwater inflow and the saline North Sea happens within these estuaries. In the NEMO model setup, the freshwater inflow is introduced at the respective river mouth points of the smooth NEMO coastline where it starts to mix with the saline North Sea water. Consequently, the simulated water at and near those points is much fresher than in reality, which leads to the low SSS bias. Note that on the one hand such a smooth coastline is necessary in NEMO to avoid numerical instabilities. On the other hand, the spatial resolution of the NEMO grid is not high enough to adequately resolve parts of the longer estuaries.

Table 6. Various metrics (see Sect. 2.7) of the simulated salinity time series in 6 m depth compared with the observations at the stations *Deutsche Bucht* and *EMS* for 2011-2018 and at *Deutsche Bucht* for 2013.

Metric	2011-2018				2013	
	<i>Deutsche Bucht</i>		<i>EMS</i>		<i>Deutsche Bucht</i>	
	HDW	HDW-BC	HDW	HDW-BC	HDW	HDW-BC
Bias [%]	-4.5	-3.7	-4	-3.6	-3.2	-1.8
Variability ratio [%]	142.7	125	151.5	136.1	82.9	74.2
Normalized RMSE [%]	40.1	34.3	51.3	47.6	36.2	27.1
Centered RMSE	0.94	0.89	0.73	0.72	0.97	0.89
Correlation	0.24	0.21	0.48	0.39	0.20	0.28

5 Summary and Conclusions

In the present study, we have introduced a methodology for the bias correction of European river runoff to provide corrected riverine inflows as forcing for ocean models in offline and coupled system model simulations. The central part of this methodology is a three-part-quantile bias correction, which can correct different biases for low, medium and high discharges. The bias correction parameters are derived in two steps. First, different correction factors for low, medium and high flows are derived for each river considered (cf. Sect. 2.5) at the location of the most downstream station for which daily discharge measurements were available. These

679 factors were then transferred to the respective river mouth on the HD model grid and to adjacent
680 coastal inflow points in its vicinity.

681 The evaluation of the bias corrected discharge at the station location showed that the bias
682 correction greatly improved the simulated discharges. For the evaluation of the bias corrected
683 discharge at the downstream station locations, we considered the mean bias and the KGE, which
684 is a quality metric combining bias, correlation and coefficient of variation. Considering the
685 same period as used to derive the bias correction factors, the mean bias is trivially close to zero.
686 However, the bias is also substantially reduced for most rivers if a different period is considered.
687 Irrespective of the period, the KGE pattern generally improves for the bias corrected discharges
688 and shows high values for many rivers. Exceptions are those rivers with a very strong
689 anthropogenic distortion of the natural flow, e.g. by many dams or large water withdrawals.
690 Here, despite of some improvements, the KGE values are still rather low, such as for the rivers
691 Dnjepr, Volga, Luleälven and a few Turkish rivers flowing into the Black Sea. The KGE also
692 shows the beneficial effect of the three-part-quantile bias correction, as correcting only the long-
693 term mean annual discharge bias is not sufficient in many areas, especially in northern Europe.
694 We found that the three-part-quantile bias correction often improves the KGE in regulated
695 rivers, so that it appears to mimic the effect of regulation, where regulation leads to the
696 elimination of peak flows while maintaining certain flow levels during low flow periods.

697 The evaluation of riverine inflows to the sea at river mouths with observed daily discharge
698 is rarely possible as there are usually no river gauges available. Even if there is a gauge at the
699 mouth of a river, the measurements are often affected by tidal influences from the coast, so that
700 the measured amounts may not represent the actual river discharge. For obvious reasons, it is
701 also difficult to compare simulated inflows with observed discharges for unmonitored rivers.
702 Therefore, we compared the simulated and bias corrected discharges with long-term mean
703 inflow estimates into different sea basins from HELCOM, OSPAR and IGC-EMO. For most of
704 the basins considered, the bias correction improves the simulated inflows. This indicates a
705 reasonable performance of the approach to transfer the bias correction factors obtained at the
706 downstream stations to the respective river mouths and adjacent coastal areas. Exceptions are
707 the Gulf of Finland, the Gulf of Riga, the Celtic Sea and the Irish Sea. For the Gulf of Finland
708 and the Celtic Sea, the deviations of the uncorrected and bias corrected inflows from the inflow
709 estimates are rather small. For the Gulf of Riga, the deviations of the uncorrected and bias
710 corrected inflows from the HELCOM estimates are also small, but they significantly
711 underestimate the IGC-EMO estimates. However, this could be due to a large overestimation
712 of the Daugava discharge during the period 1995-2019 in the IGC-EMO data and thus also of
713 the corresponding Gulf of Riga inflow. For the Irish Sea, IGC-EMO seems to be closer to reality
714 as the OSPAR inflow does not cover the unmonitored rivers in the British part of the catchment.

715 A caveat applies for rivers where the human influence on river flow has changed
716 significantly over time. Applying bias correction factors derived for 1979-2014 to earlier
717 periods may lead to errors for regulated rivers in years before these regulatory measures were
718 implemented. This is the case for the Ebro, where irrigation activities have largely intensified
719 during the period 1979-2014 compared to earlier periods (see Sect. 3.3). A detailed analysis of
720 the rivers and periods concerned is beyond the scope of this study. However, at least for the
721 period 1950-1978, the KGE distribution does not seem to be significantly affected, as there is
722 no noticeable deterioration.

723 We have shown that our bias correction method works well for Europe at the station
724 locations as well as for the riverine inflow into northern and western European sea basins. Using

725 two NEMO simulations in the German Bight, we have also shown that the use of the bias
726 corrected discharges as forcing leads to an improved simulation of sea surface salinity in coastal
727 areas especially regarding the mean salinity and its variability. However, for the potential
728 transfer of the bias correction methodology to other regions, it has to be pointed out that the
729 application of the ~~three-part-quantile~~ bias correction over a region only makes sense if a large
730 part of the catchment area is covered by available daily discharge measurements. As the ~~three-~~
731 ~~part-quantile~~ bias correction is based on biases in three percentile ranges of daily flows, it is
732 also suitable for the use in climate change applications. Here the bias correction factors can be
733 derived from a historical discharge simulation and then applied to future projections or past
734 reconstructions. In addition, the bias correction can also be applied in ~~rRegional C~~coupled
735 ~~Ssystem mModel (RCSM)~~simulations, where the bias correction factors can be derived from
736 an initial simulation and then applied during the run-time of the actual ~~RCSM-coupled~~
737 simulation. This capability has been implemented in the HD model v5.2.2 (Hagemann et al.,
738 2023) and is currently being applied in the coupled system model GCOAST-GCOAST-AHOI
739 ~~system~~-(Ho-Hagemann et al., 2020).- Finally, we note that the bias corrected discharges are
740 available from the World Data Centre for Climate and are already used within the
741 CoastalFutures project (<https://www.coastalfutures.de>).

742 **Data Availability Statement**

743 Many of the observed daily discharge data used can be obtained from the Global Runoff Data
744 Centre (https://grdc.bafg.de/GRDC/EN/02_srvcs/21_tmsrs/riverdischarge_node.html). Other
745 data have been retrieved from public websites associated with the sources referred to in Sect.
746 2.5. GSWP3 data were retrieved from the ISIMIP data portal (<https://data.isimip.org>) and
747 WFDE5 data were retrieved from the Copernicus Climate Data Store
748 (<https://cds.climate.copernicus.eu>). OSPAR data were taken from an OSPAR report (Farkas
749 and Skarbøvik, 2021) or its associated data available on the OSPAR webpage
750 (<https://odims.ospar.org/en/search/?dataset=rid-data-reports>). This study has been conducted
751 using E.U. Copernicus Marine Service Information data on SSS ([https://doi.org/10.48670/moi-](https://doi.org/10.48670/moi-00051)
752 00051) and some French discharge measurements. The daily data of surface runoff and
753 subsurface runoff as well as the simulated and bias corrected discharge data (Hagemann and
754 Stacke, 2023) can be accessed via the World Data Centre for Climate-~~(WDCC)~~ at the German
755 Climate Computing CenterDKRZ.

756 **Acknowledgments**

757 This study was conducted within the CoastalFutures project that was funded by the German
758 Federal Ministry of Education and Research under grant number 03F0911E. TN was supported
759 by the subproject ‘A6 - The earth system variability and predictability in changing climate’ of
760 Germany’s Excellence Strategy EXC 2037 ‘CLICCS - Climate, Climatic Change, and Society’
761 with project no. 390683824, funded by the Deutsche Forschungsgemeinschaft (~~DFG~~, German
762 Research Foundation). We thank the German Climate Computing CenterDKRZ for providing
763 the computing resources to perform the HD simulations. We acknowledge the Copernicus
764 Climate Data Store and the ISIMIP project for making WFDE5 and GSWP3 datasets available.
765 We are deeply indebted to all data providers. We are also grateful to Sonja van Leuwen (Royal
766 Netherlands Institute for Sea Research) for providing us with the latest version of the IGC-
767 EMO data. We are thankful to Sebastian Grayek (Helmholtz-Zentrum Hereon) for the
768 discussion on his NEMO results using an initial version of the bias corrected discharges.
769 Finally, we thank Tobias Stacke (Max Planck Institute for Meteorology) for conducting the
770 HydroPy simulations published in Hagemann and Stacke (2023).

771 **Author Contributions**

772 SH developed and applied the three-part-quantile bias correction, conducted the discharge
773 simulations and analysis of results, and wrote the manuscript. HH conducted the NEMO
774 simulations, helped with the analysis of results and revised the manuscript. TN evaluated the
775 SSS data of the NEMO simulations, helped with the analysis of results and revised the
776 manuscript.

777 **Conflict of Interest Statement**

778 The authors declare that the research was conducted in the absence of any commercial or
779 financial relationships that could be construed as a potential conflict of interest.

780 **References**

781

- 782 Arora, V. K., Seiler, C., Wang, L. B., and Kou-Giesbrecht, S.: Towards an ensemble-based
783 evaluation of land surface models in light of uncertain forcings and observations,
784 *Biogeosci.*, 20, 1313-1355, <https://doi.org/10.5194/bg-20-1313-2023>, 2023.
- 785 Becker, G. A., Dick, S., and Dippner, J. W.: Hydrography of the German Bight, *Mar. Ecol.*
786 *Prog. Ser.*, 91, 9-18, <https://doi.org/10.3354/meps091009>, 1992.
- 787 Becker, G. A., Giese, H., Isert, K., König, P., Langenberg, H., Pohlmann, T., and Schrum, C.:
788 Mesoscale structures, fluxes and water mass variability in the German Bight as exemplified
789 in the KUSTOS- experiments and numerical models, *Deutsche Hydrographische*
790 *Zeitschrift*, 51, 155-179, <https://doi.org/10.1007/bf02764173>, 1999.
- 791 Borgvang, S. A., Skarbøvik, E., and Pengerud, A.: RID 2006 data report: Presentation and
792 Assessment of the OSPAR Contracting Parties' RID 2006 Data., Norwegian Institute for
793 Agricultural and Environmental Research, London, No. 376/2008, 373 pp., 2008.
- 794 Brown, J. D., and Seo, D. J.: A nonparametric postprocessor for bias correction of
795 hydrometeorological and hydrologic ensemble forecasts, *J. Hydrometeorol.*, 11, 642-665,
796 <https://doi.org/10.1175/2009jhm1188.1>, 2010.
- 797 Brown, J. D., and Seo, D. J.: Evaluation of a nonparametric post-processor for bias correction
798 and uncertainty estimation of hydrologic predictions, *Hydrol. Process.*, 27, 83-105,
799 <https://doi.org/10.1002/hyp.9263>, 2012.
- 800 Budhathoki, A., Tanaka, T., and Tachikawa, Y.: Correcting streamflow bias considering its
801 spatial structure for impact assessment of climate change on floods using d4PDF in the
802 Chao Phraya River Basin, Thailand, *J. Hydrol.-Reg. Stud.*, 42,
803 <https://doi.org/10.1016/j.ejrh.2022.101150>, 2022.
- 804 Cannon, A. J., Sobie, S. R., and Murdock, T. Q.: Bias correction of GCM precipitation by
805 quantile mapping: How well do methods preserve changes in quantiles and extremes?, *J*
806 *Climate*, 28, 6938-6959, <https://doi.org/10.1175/Jcli-D-14-00754.1>, 2015.
- 807 Compo, G. P., Whitaker, J. S., Sardeshmukh, P. D., Matsui, N., Allan, R. J., Yin, X., Gleason,
808 B. E., Vose, R. S., Rutledge, G., Bessemoulin, P., Bronnimann, S., Brunet, M.,
809 Crouthamel, R. I., Grant, A. N., Groisman, P. Y., Jones, P. D., Kruk, M. C., Kruger, A. C.,
810 Marshall, G. J., Maugeri, M., Mok, H. Y., Nordli, O., Ross, T. F., Trigo, R. M., Wang, X.
811 L., Woodruff, S. D., and Worley, S. J.: The Twentieth Century Reanalysis Project, *Q. J.*
812 *Roy. Meteor. Soc.*, 137, 1-28, <https://doi.org/10.1002/qj.776>, 2011.
- 813 Cucchi, M., Weedon, G. P., Amici, A., Bellouin, N., Lange, S., Schmied, H. M., Hersbach,
814 H., and Buontempo, C.: WFDE5: bias-adjusted ERA5 reanalysis data for impact studies,

815 Earth Syst. Sci. Data, 12, 2097–2120-2097–2120, <https://doi.org/10.5194/essd-12-2097->
816 [2020](https://doi.org/10.5194/essd-12-2097-2020), 2020.

817 Daewel, U., and Schrum, C.: Low-frequency variability in North Sea and Baltic Sea identified
818 through simulations with the 3-D coupled physical–biogeochemical model ECOSMO,
819 Earth Syst. Dyn., 8, 801-801, <https://doi.org/10.5194/esd-8-801-2017>, 2017.

820 Daraio, J. A.: Hydrologic Model Evaluation and Assessment of Projected Climate Change
821 Impacts Using Bias-Corrected Stream Flows, Water, 12,
822 <https://doi.org/10.3390/w12082312>, 2020.

823 Dirmeyer, P. A., Gao, X., Zhao, M., Guo, Z., Oki, T., and Hanasaki, N.: GSWP-2:
824 Multimodel Analysis and Implications for Our Perception of the Land Surface, Bull. Amer,
825 Meteor. Soc., 87, 1381-1398, <https://doi.org/10.1175/bams-87-10-1381>, 2006.

826 Droghei, R., Buongiorno Nardelli, B., and Santoleri, R.: A New Global Sea Surface Salinity
827 and Density Dataset From Multivariate Observations (1993–2016), Front. Mar. Sci., 5,
828 <https://doi.org/10.3389/fmars.2018.00084>, 2018.

829 Farkas, C., and Skarbøvik, E.: OSPAR Contracting Parties’ RID 2019 Data Report, NIBIO –
830 Norwegian Institute for Bioeconomy Research, 57 pp., 2021.

831 Farmer, W. H., Over, T. M., and Kiang, J. E.: Bias correction of simulated historical daily
832 streamflow at ungauged locations by using independently estimated flow duration curves,
833 Hydrol. Earth Syst. Sci., 22, 5741-5758, <https://doi.org/10.5194/hess-22-5741-2018>, 2018.

834 Gupta, H. V., Kling, H., Yilmaz, K. K., and Martinez, G. F.: Decomposition of the mean
835 squared error and NSE performance criteria: Implications for improving hydrological
836 modelling, J. Hydrol., 377, 80–91-80–91, <https://doi.org/10.1016/j.jhydrol.2009.08.003>,
837 2009.

838 Haddeland, I., Clark, D. B., Franssen, W., Ludwig, F., Voß, F., Arnell, N. W., Bertrand, N.,
839 Best, M., Folwell, S., Gerten, D., Gomes, S., Gosling, S. N., Hagemann, S., Hanasaki, N.,
840 Harding, R., Heinke, J., Kabat, P., Koirala, S., Oki, T., Polcher, J., Stacke, T., Viterbo, P.,
841 Weedon, G. P., and Yeh, P.: Multimodel estimate of the global terrestrial water balance:
842 setup and first results, J. Hydrometeorol., 12, 869-884,
843 <https://doi.org/10.1175/2011jhm1324.1>, 2011.

844 Hagemann, S., Stacke, T., and Ho-Hagemann, H. T. M.: High Resolution Discharge
845 Simulations Over Europe and the Baltic Sea Catchment, Front. Earth Sci., 8,
846 <https://doi.org/10.3389/feart.2020.00012>, 2020.

847 Hagemann, S., and Stacke, T.: Complementing ERA5 and E-OBS with high-resolution river
848 discharge over Europe, Oceanologia, 65, 230-248,
849 <https://doi.org/10.1016/j.oceano.2022.07.003>, 2022.

850 Hagemann, S., Ho-Hagemann, H. T. M., and Hanke, M.: The Hydrological Discharge Model -
851 a river runoff component for offline and coupled model applications. Zenodo.
852 <https://doi.org/10.5281/zenodo.10405875>, 2023.

853 Hagemann, S., and Stacke, T.: Bias corrected high resolution river runoff over Europe. World
854 Data Center for Climate (WDCC) at DKRZ.
855 https://doi.org/10.26050/WDCC/Biasc_hr_riverro_Eu, 2023.

856 Hassler, B., and Lauer, A.: Comparison of reanalysis and observational precipitation datasets
857 including ERA5 and WFDE5, Atmos., 12, <https://doi.org/10.3390/atmos12111462>, 2021.

858 HELCOM: The Third Baltic Sea Pollution Load Compilation, Balt. Sea Environ. Proc., no 70,
859 Baltic Marine Environment Protection Commission--Helsinki Commission, Helsinki,
860 Finland, 134 p. pp., 1998.

861 Hersbach, H., Bell, B., Berrisford, P., Hirahara, S., Horányi, A., Muñoz-Sabater, J. n.,
862 Nicolas, J., Peubey, C., Radu, R., Schepers, D., Simmons, A., Soci, C., Abdalla, S.,
863 Abellan, X., Balsamo, G., Bechtold, P., Biavati, G., Bidlot, J., Bonavita, M., Chiara, G.,

864 Dahlgren, P., Dee, D., Diamantakis, M., Dragani, R., Flemming, J., Forbes, R., Fuentes,
865 M., Geer, A., Haimberger, L., Healy, S., Hogan, R. J., Hólm, E. a., Janisková, M., Keeley,
866 S., Laloyaux, P., Lopez, P., Lupu, C., Radnoti, G., Rosnay, P., Rozum, I., Vamborg, F.,
867 Villaume, S., and Thépaut, J.-N.: The ERA5 global reanalysis, *Quart. J. Roy. Meteor. Soc.*,
868 146, 1999-2049, <https://doi.org/10.1002/qj.3803>, 2020.

869 Ho-Hagemann, H. T. M., Hagemann, S., Grayek, S., Petrik, R., Rockel, B., Staneva, J., Feser,
870 F., and Schrum, C.: Internal Model Variability of the Regional Coupled System Model
871 GCOAST-AHOI, *Atmos.*, 11, 227-227, <https://doi.org/10.3390/atmos11030227>, 2020.

872 Hordoir, R., Polcher, J., Brun-Cottan, J. C., and Madec, G.: Towards a parametrization of
873 river discharges into ocean general circulation models: a closure through energy
874 conservation, *Clim. Dyn.*, 31, 891-908, <https://doi.org/10.1007/s00382-008-0416-4>, 2008.

875 Hordoir, R., and Meier, H. E. M.: Freshwater fluxes in the Baltic Sea: A model study, *J.*
876 *Geophys. Res.*, 115, C08028-C08028, <https://doi.org/10.1029/2009jc005604>, 2010.

877 ISIMIP: ISIMIP2a Simulation protocol (extended version):
878 https://www.isimip.org/documents/647/ISIMIP2a_protocol_230302.pdf, access: 8.3.,
879 2023.

880 Kim, H.: Global Soil Wetness Project Phase 3 Atmospheric Boundary Conditions
881 (Experiment 1). Data Integration and Analysis System (DIAS).
882 <https://doi.org/10.20783/DIAS.501>, 2017.

883 Kim, K. B., Kwon, H. H., and Han, D. W.: Bias-correction schemes for calibrated flow in a
884 conceptual hydrological model, *Hydrol. Res.*, 52, 196-211,
885 <https://doi.org/10.2166/nh.2021.043>, 2021.

886 Klein, H., and Frohse, A.: Oceanographic Processes in the German Bight, Heide, Holstein:
887 Boyens, 60-76, 2008.

888 Kling, H., Fuchs, M., and Paulin, M.: Runoff conditions in the upper Danube basin under an
889 ensemble of climate change scenarios, *J. Hydrol.*, 424-425, 264-277-264-277,
890 <https://doi.org/10.1016/j.jhydrol.2012.01.011>, 2012.

891 Knoben, W. J. M., Freer, J. E., and Woods, R. A.: Technical note: Inherent benchmark or not?
892 Comparing Nash-Sutcliffe and Kling-Gupta efficiency scores, *Hydrol. Earth Syst. Sci.*, 23,
893 4323-4331, <https://doi.org/10.5194/hess-23-4323-2019>, 2019.

894 Krzysztofowicz, R., and Maranzano, C. J.: Hydrologic uncertainty processor for probabilistic
895 stage transition forecasting, *J Hydrol*, 293, 57-73,
896 <https://doi.org/10.1016/j.jhydrol.2004.01.003>, 2004.

897 Lehmann, A., and Hinrichsen, H.-H.: On the thermohaline variability of the Baltic Sea, *J.*
898 *Mar. Syst.*, 25, 333-357, [https://doi.org/10.1016/s0924-7963\(00\)00026-9](https://doi.org/10.1016/s0924-7963(00)00026-9), 2000.

899 Lenhart, H. J., Mills, D. K., Baretta-Bekker, H., van Leeuwen, S. M., van der Molen, J.,
900 Baretta, J. W., Blaas, M., Desmit, X., Kuhn, W., Lacroix, G., Los, H. J., Menesguen, A.,
901 Neves, R., Proctor, R., Ruardij, P., Skogen, M. D., Vanhoutte-Brunier, A., Villars, M. T.,
902 and Wakelin, S. L.: Predicting the consequences of nutrient reduction on the eutrophication
903 status of the North Sea, *J. Mar. Syst.*, 81, 148-170,
904 <https://doi.org/10.1016/j.jmarsys.2009.12.014>, 2010.

905 Madadgar, S., Moradkhani, H., and Garen, D.: Towards improved post-processing of
906 hydrologic forecast ensembles, *Hydrol. Process.*, 28, 104-122,
907 <https://doi.org/10.1002/hyp.9562>, 2014.

908 Madec, G., Bourdallé-Badie, R., Bouffier, P.-A., Bricaud, C., Bruciaferr, D., Calvert, D.,
909 Chanut, J., Clementi, E., Coward, A., Delrosso, D., Ethé, C., Flavoni, S., Graham, T.,
910 Harle, J., Iovino, D., Lea, D., Lévy, C., Lovato, T., Martin, N., and Vancoppenolle, M.:
911 NEMO ocean engine. Notes du Pôle de modélisation de l'Institut Pierre-Simon Laplace
912 (IPSL), 27, Zenodo, <https://doi.org/10.5281/zenodo.3248739>, 2017.

913 Malek, K., Reed, P., Zeff, H., Hamilton, A., Wrzesien, M., Holtzman, N., Steinschneider, S.,
914 Herman, J., and Pavelsky, T.: Bias correction of hydrologic projections strongly impacts
915 inferred climate vulnerabilities in institutionally complex water systems, *J. Water Res.*
916 *Plan. Man.*, 148, [https://doi.org/10.1061/\(Asce\)Wr.1943-5452.0001493](https://doi.org/10.1061/(Asce)Wr.1943-5452.0001493), 2022.

917 Maraun, D., Shepherd, T. G., Widmann, M., Zappa, G., Walton, D., Gutiérrez, J. M.,
918 Hagemann, S., Richter, I., Soares, P. M. M., Hall, A., and Mearns, L. O.: Towards process-
919 informed bias correction of climate change simulations, *Nat Clim Change*, 7, 764-773,
920 <https://doi.org/10.1038/Nclimate3418>, 2017.

921 Marzeion, B., Levermann, A., and Mignot, J.: The Role of Stratification-Dependent Mixing
922 for the Stability of the Atlantic Overturning in a Global Climate Model*, *J. Phys.*
923 *Oceanogr.*, 37, 2672–2681-2672–2681, <https://doi.org/10.1175/2007jpo3641.1>, 2007.

924 Mengel, M., Treu, S., Lange, S., and Frieler, K.: ATTRICI v1.1-counterfactual climate for
925 impact attribution, *Geosci Model Dev*, 14, 5269-5284, [https://doi.org/10.5194/gmd-14-](https://doi.org/10.5194/gmd-14-5269-2021)
926 [5269-2021](https://doi.org/10.5194/gmd-14-5269-2021), 2021.

927 Merchán, D., Causapé, J., and Abrahao, R.: Impact of irrigation implementation on hydrology
928 and water quality in a small agricultural basin in Spain, *Hydrol. Sci. J.*, 58, 1400–1413-
929 1400–1413, 2013.

930 Nguyen, T. T., Staneva, J., Grayek, S., Bonaduce, A., Hagemann, S., Pham, N. T., Kumar, R.,
931 and Rakovec, O.: Impacts of extreme river discharge on coastal dynamics and
932 environment: Insights from high-resolution modeling in the German Bight, *Reg. Stud.*
933 *Mar. Sci.*, 73, <https://doi.org/10.1016/j.rsma.2024.103476>, 2024.

934 Piani, C., Weedon, G. P., Best, M., Gomes, S. M., Viterbo, P., Hagemann, S., and Haerter, J.
935 O.: Statistical bias correction of global simulated daily precipitation and temperature for
936 the application of hydrological models, *J Hydrol*, 395, 199-215,
937 <https://doi.org/10.1016/j.jhydrol.2010.10.024>, 2010.

938 Shi, X. G., Wood, A. W., and Lettenmaier, D. P.: How Essential is Hydrologic Model
939 Calibration to Seasonal Streamflow Forecasting?, *J. Hydrometeorol.*, 9, 1350-1363,
940 <https://doi.org/10.1175/2008jhm1001.1>, 2008.

941 Stacke, T., and Hagemann, S.: HydroPy (v1.0): A new global hydrology model written in
942 Python, *Geosci. Model Dev.*, <https://doi.org/10.5194/gmd-2021-53>, 2021.

943 Taylor, K. E.: Summarizing multiple aspects of model performance in a single diagram., *J*
944 *Geophys Res-Atmos*, 106, 7183-7192, [https://doi.org/Doi 10.1029/2000jd900719](https://doi.org/Doi%2010.1029/2000jd900719), 2001.

945 Teutschbein, C., and Seibert, J.: Bias correction of regional climate model simulations for
946 hydrological climate-change impact studies: Review and evaluation of different methods, *J*
947 *Hydrol*, 456-457, 12-29, <https://doi.org/10.1016/j.jhydrol.2012.05.052>, 2012.

948 Väli, G., Meier, H. E. M., and Elken, J.: Simulated halocline variability in the Baltic Sea and
949 its impact on hypoxia during 1961-2007, *J. Geophys. Res. Oceans*, 118, 6982–7000-6982–
950 7000, <https://doi.org/10.1002/2013jc009192>, 2013.

951 Van Leeuwen, S., and Lenhart, H. J.: OSPAR ICG-EMO riverine database 2020-05-01 used
952 in 2020 workshop. NIOZ, V1. <https://doi.org/10.25850/nioz/7b.b.vc>, 2021.

953 Van Leeuwen, S., and Hagemann, S.: Mapping of IGC-EMO nutrient loads on the high
954 resolution HD model grid (Version 1). World Data Center for Climate (WDCC) at DKRZ.
955 https://doi.org/10.26050/WDCC/IGC-EMO_HD_v1, 2023.

956 Vinayachandran, P. N., Jahfer, S., and Nanjundiah, R. S.: Impact of river runoff into the ocean
957 on Indian summer monsoon, *Environ. Res. Lett.*, 10, [https://doi.org/10.1088/1748-](https://doi.org/10.1088/1748-9326/10/5/054008)
958 [9326/10/5/054008](https://doi.org/10.1088/1748-9326/10/5/054008), 2015.

959 Warszawski, L., Frieler, K., Huber, V., Piontek, F., Serdeczny, O., and Schewe, J.: The Inter-
960 Sectoral Impact Model Intercomparison Project (ISI-MIP): Project framework, *Proc. Natl.*
961 *Acad. Sci. USA*, 111, 3228-3232, <https://doi.org/10.1073/pnas.1312330110>, 2014.

- 962 Weedon, G. P., Gomes, S., Viterbo, P., Shuttleworth, W. J., Blyth, E., Österle, H., Adam, J.
963 C., Bellouin, N., Boucher, O., and Best, M.: Creation of the WATCH Forcing Data and Its
964 Use to Assess Global and Regional Reference Crop Evaporation over Land during the
965 Twentieth Century, *J. Hydrometeorol.*, 12, 823-848,
966 <https://doi.org/10.1175/2011JHM1369.1>, 2011.
- 967 Yoshimura, K., and Kanamitsu, M.: Dynamical global downscaling of global reanalysis, *Mon.*
968 *Weather Rev.*, 136, 2983-2998, <https://doi.org/10.1175/2008mwr2281.1>, 2008.
- 969 Zhao, L., Duan, Q., Schaake, J., Ye, A., and Xia, J.: A hydrologic post-processor for ensemble
970 streamflow predictions, *Adv. Geosci.*, 29, 51-59, [https://doi.org/10.5194/adgeo-29-51-](https://doi.org/10.5194/adgeo-29-51-2011)
971 [2011](https://doi.org/10.5194/adgeo-29-51-2011), 2011.
- 972 Zuo, H., Balmaseda, M. A., Tietsche, S., Mogensen, K., and Mayer, M.: The ECMWF
973 operational ensemble reanalysis–analysis system for ocean and sea ice: a description of the
974 system and assessment, *Ocean Sci.*, 15, 779-808, <https://doi.org/10.5194/os-15-779-2019>,
975 2019.

976

977

978 **Supplementary Material**

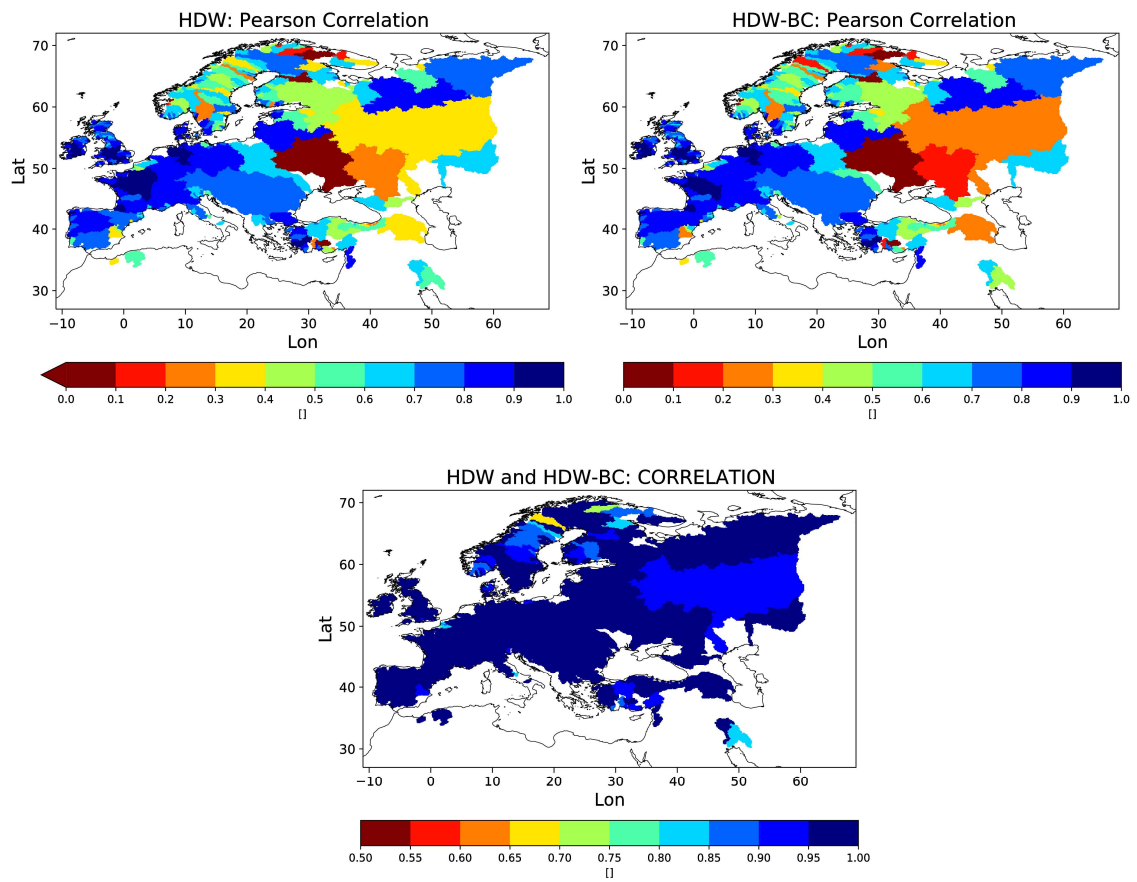
979 **Table S1:** Various metrics (see Sect. 2.7) of the simulated salinity time series in 6 m
 980 depth compared with the SSS data of Droghei et al. (2018) at the locations of the
 981 stations *Deutsche Bucht* and *EMS* for 2011-2018 and at *Deutsche Bucht* for 2013.

Metric	2011-2018				2013	
	<i>Deutsche Bucht</i>		<i>EMS</i>		<i>Deutsche Bucht</i>	
	HDW	HDW-BC	HDW	HDW-BC	HDW	HDW-BC
Bias [%]	<u>-3</u>	<u>-2.2</u>	<u>-1.1</u>	<u>-0.7</u>	<u>-3.9</u>	<u>-2.6</u>
Variability ratio [%]	<u>135.5</u>	<u>117.1</u>	<u>130.4</u>	<u>116.7</u>	<u>132.7</u>	<u>116.2</u>
Normalized RMSE [%]	<u>23.2</u>	<u>18.7</u>	<u>25.6</u>	<u>22.9</u>	<u>50.8</u>	<u>36.9</u>
Centered RMSE	<u>1.01</u>	<u>0.89</u>	<u>0.91</u>	<u>0.84</u>	<u>0.78</u>	<u>0.70</u>
Correlation	<u>0.14</u>	<u>0.21</u>	<u>0.25</u>	<u>0.26</u>	<u>0.16</u>	<u>0.22</u>

982

983

984



985
986

987

988

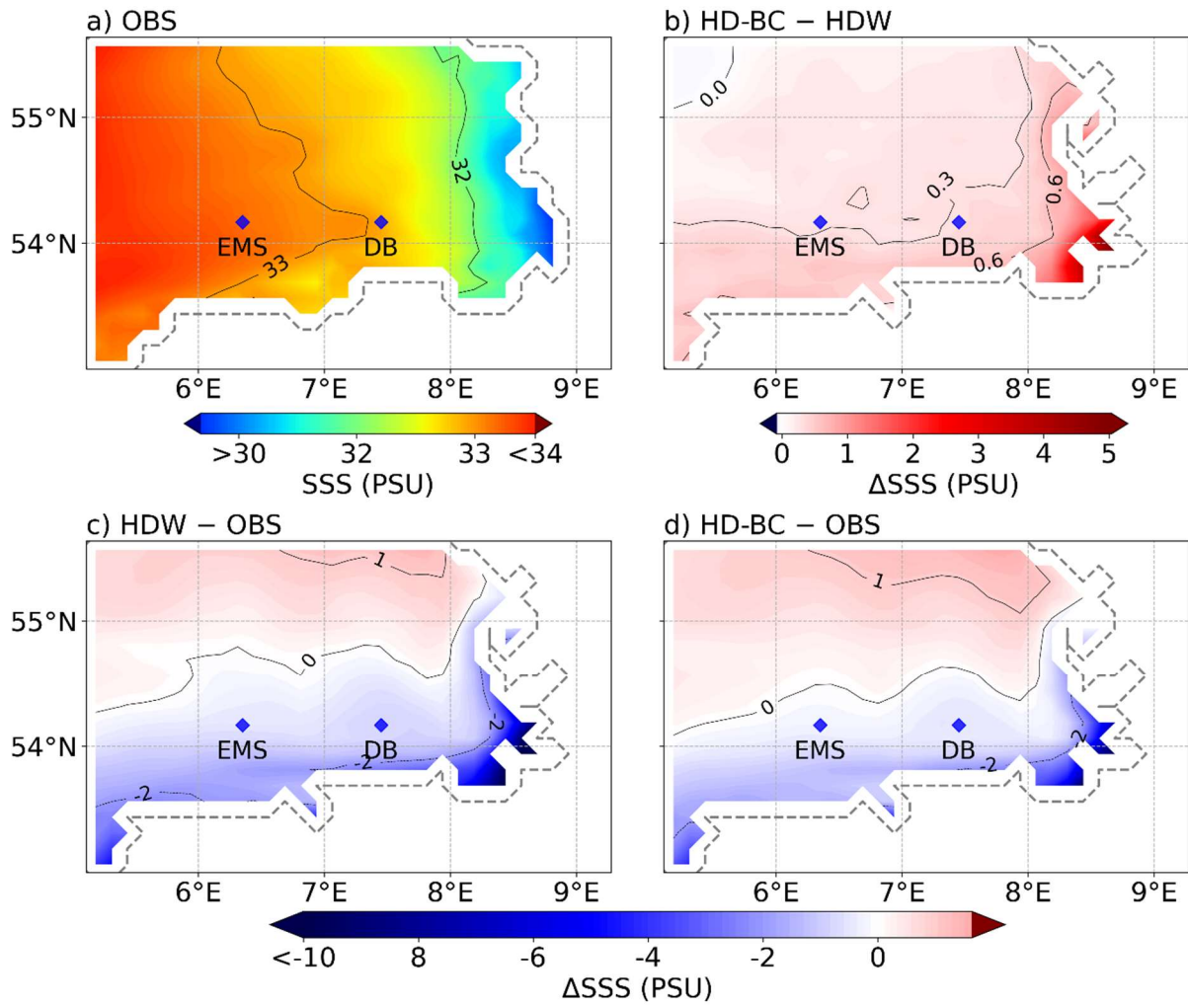
989

990

991

Figure S1: Correlation of a) HDW and b) HDW-BC with observations as well as c) HDW with HDW-BC from 1979-2014.

992



993

994

Figure S2. Same as Figure 13, but with SSS averages calculated over the period June 2013.

995

996